Statistical Complexity and Fisher-Shannon Information. Applications

ARTICLE · JANUARY 2012

DOI: 10.1007/978-90-481-3890-6_4 · Source: arXiv

4 AUTHORS, INCLUDING:

Ricardo Lopez-Ruiz
Univ. of Zaragoza, Spain
95 PUBLICATIONS **1,176** CITATIONS

SEE PROFILE

Xavier Calbet
University of Zaragoza
82 PUBLICATIONS **887** CITATIONS

SEE PROFILE

Chapter 4
Statistical Complexity and Fisher-Shannon Information: Applications

Ricardo López-Ruiz, Jaime Sañudo, Elvira Romera, and Xavier Calbet

Abstract In this chapter, a statistical measure of complexity and the Fisher-Shannon information product are introduced and their properties are discussed. These measures are based on the interplay between the Shannon information, or a function of it, and the separation of the set of accessible states to a system from the equiprobability distribution, i.e. the disequilibrium or the Fisher information, respectively. Different applications in discrete and continuous systems are shown. Some of them are concerned with quantum systems, from prototypical systems such as the H-atom, the harmonic oscillator and the square well to other ones such as He-like ions, Hooke's atoms or just the periodic table. In all of them, these statistical indicators show an interesting behavior able to discern and highlight some conformational properties of those systems.

4.1 A Statistical Measure of Complexity. Some Applications

This century has been told to be the century of *complexity* [1]. Nowadays the question *"what is complexity?"* is circulating over the scientific crossroads of physics, biology, mathematics and computer science, although under the present understanding of the world could be no urgent to answer this question. However, many different points of view have been developed to this respect and hence a lot of different answers can be found in the literature. Here we explain in detail one of these options.

On the most basic grounds, an object, a procedure, or system is said to be "complex" when it does not match patterns regarded as simple. This sounds rather like an oxymoron but common knowledge tells us what is simple and complex: simplified systems or idealizations are always a starting point to solve scientific problems. The notion of "complexity" in physics [2, 3] starts by considering the perfect crystal

R. López-Ruiz (✉)
Department of Computer Science, Faculty of Science and BIFI, University of Zaragoza, Zaragoza 50009, Spain
e-mail: rilopez@unizar.es

K.D. Sen (ed.), *Statistical Complexity*,
DOI 10.1007/978-90-481-3890-6_4,

and the isolated ideal gas as examples of simple models and therefore as systems with zero "complexity". Let us briefly recall their main characteristics with "order", "information" and "equilibrium".

A perfect crystal is completely ordered and the atoms are arranged following stringent rules of symmetry. The probability distribution for the states accessible to the perfect crystal is centered around a prevailing state of perfect symmetry. A small piece of "information" is enough to describe the perfect crystal: the distances and the symmetries that define the elementary cell. The "information" stored in this system can be considered minimal. On the other hand, the isolated ideal gas is completely disordered. The system can be found in any of its accessible states with the same probability. All of them contribute in equal measure to the "information" stored in the ideal gas. It has therefore a maximum "information". These two simple systems are extrema in the scale of "order" and "information". It follows that the definition of "complexity" must not be made in terms of just "order" or "information".

It might seem reasonable to propose a measure of "complexity" by adopting some kind of distance from the equiprobable distribution of the accessible states of the system. Defined in this way, "disequilibrium" would give an idea of the probabilistic hierarchy of the system. "Disequilibrium" would be different from zero if there are privileged, or more probable, states among those accessible. But this would not work. Going back to the two examples we began with, it is readily seen that a perfect crystal is far from an equidistribution among the accessible states because one of them is totally prevailing, and so "disequilibrium" would be maximum. For the ideal gas, "disequilibrium" would be zero by construction. Therefore such a distance or "disequilibrium" (a measure of a probabilistic hierarchy) cannot be directly associated with "complexity".

In Fig. 4.1 we sketch an intuitive qualitative behavior for "information" H and "disequilibrium" D for systems ranging from the perfect crystal to the ideal gas. This graph suggests that the product of these two quantities could be used as a measure of "complexity": $C = H \cdot D$. The function C has indeed the features and asymtotical properties that one would expect intuitively: it vanishes for the perfect crystal and for the isolated ideal gas, and it is different from zero for the rest of the systems of particles. We will follow these guidelines to establish a quantitative measure of "complexity".

Before attempting any further progress, however, we must recall that "complexity" cannot be measured univocally, because it depends on the nature of the description (which always involves a reductionist process) and on the scale of observation. Let us take an example to illustrate this point. A computer chip can look very different at different scales. It is an entangled array of electronic elements at microscopic scale but only an ordered set of pins attached to a black box at a macroscopic scale.

We shall now discuss a measure of "complexity" based on the statistical description of systems. Let us assume that the system has N accessible states $\{x_1, x_2, \ldots, x_N\}$ when observed at a given scale. We will call this an N-system.

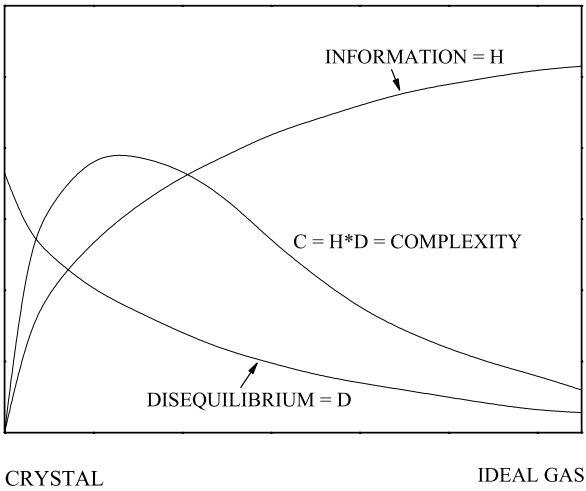

Fig. 4.1 Sketch of the intuitive notion of the magnitudes of "information" (H) and "disequilibrium" (D) for the physical systems and the behavior intuitively required for the magnitude "complexity". The quantity $C = H \cdot D$ is proposed to measure such a magnitude

Our understanding of the behavior of this system determines the corresponding probabilities $\{p_1, p_2, \ldots, p_N\}$ (with the condition $\sum_{i=1}^{N} p_i = 1$) of each state ($p_i > 0$ for all i). Then the knowledge of the underlying physical laws at this scale is incorporated into a probability distribution for the accessible states. It is possible to find a quantity measuring the amount of "information". Under to the most elementary conditions of consistency, Shannon [4] determined the unique function $H(p_1, p_2, \ldots, p_N)$ that accounts for the "information" stored in a system:

$$H = -K \sum_{i=1}^{N} p_i \log p_i, \tag{4.1}$$

where K is a positive constant. The quantity H is called *information*. The redefinition of information H as some type of monotone function of the Shannon entropy can be also useful in many contexts as we shall show in the next sections. In the case of a crystal, a state x_c would be the most probable $p_c \sim 1$, and all others x_i would be very improbable, $p_i \sim 0$, $i \neq c$. Then $H_c \sim 0$. On the other side, equiprobability characterizes an isolated ideal gas, $p_i \sim 1/N$ so $H_g \sim K \log N$, i.e., the maximum of information for a N-system. (Notice that if one assumes equiprobability and $K = \kappa \equiv$ *Boltzmann constant*, H is identified with the thermodynamic entropy, $S = \kappa \log N$). Any other N-system will have an amount of information between those two extrema.

Let us propose a definition of *disequilibrium* D in a N-system [5]. The intuitive notion suggests that some kind of distance from an equiprobable distribution should be adopted. Two requirements are imposed on the magnitude of D: $D > 0$ in order to have a positive measure of "complexity" and $D = 0$ on the limit of equiprobability.

The straightforward solution is to add the quadratic distances of each state to the equiprobability as follows:

$$D = \sum_{i=1}^{N} \left(p_i - \frac{1}{N} \right)^2 . \tag{4.2}$$

According to this definition, a crystal has maximum disequilibrium (for the dominant state, $p_c \sim 1$, and $D_c \to 1$ for $N \to \infty$) while the disequilibrium for an ideal gas vanishes ($D_g \sim 0$) by construction. For any other system D will have a value between these two extrema.

We now introduce the definition of *complexity* C of a N-system [6, 7]. This is simply the interplay between the information stored in the system and its disequilibrium:

$$C = H \cdot D = - \left(K \sum_{i=1}^{N} p_i \log p_i \right) \cdot \left(\sum_{i=1}^{N} \left(p_i - \frac{1}{N} \right)^2 \right) . \tag{4.3}$$

This definition fits the intuitive arguments. For a crystal, disequilibrium is large but the information stored is vanishingly small, so $C \sim 0$. On the other hand, H is large for an ideal gas, but D is small, so $C \sim 0$ as well. Any other system will have an intermediate behavior and therefore $C > 0$.

As was intuitively suggested, the definition of complexity (4.3) also depends on the *scale*. At each scale of observation a new set of accessible states appears with its corresponding probability distribution so that complexity changes. Physical laws at each level of observation allow us to infer the probability distribution of the new set of accessible states, and therefore different values for H, D and C will be obtained. The straightforward passage to the case of a continuum number of states, x, can be easily inferred. Thus we must treat with probability distributions with a continuum support, $p(x)$, and normalization condition $\int_{-\infty}^{+\infty} p(x)dx = 1$. Disequilibrium has the limit $D = \int_{-\infty}^{+\infty} p^2(x)dx$ and the complexity could be defined by:

$$C = H \cdot D = - \left(K \int_{-\infty}^{+\infty} p(x) \log p(x) dx \right) \cdot \left(\int_{-\infty}^{+\infty} p^2(x) dx \right) . \tag{4.4}$$

As we shall see, other possibilities for the continuous extension of C are also possible.

Direct simulations of the definition give the values of C for general N-systems. The set of all the possible distributions $\{p_1, p_2, \ldots, p_N\}$ where an N-system could be found is sampled. For the sake of simplicity H is normalized to the interval $[0, 1]$. Thus $H = \sum_{i=1}^{N} p_i \log p_i / \log N$. For each distribution $\{p_i\}$ the normalized information $H(\{p_i\})$, and the disequilibrium $D(\{p_i\})$ (4.2) are calculated. In each case the normalized complexity $C = H \cdot D$ is obtained and the pair (H, C) stored. These two magnitudes are plotted on a diagram $(H, C(H))$ in order to verify the qualitative behavior predicted in Fig. 4.1. For $N = 2$ an analytical expression for the curve $C(H)$ is obtained. If the probability of one state is $p_1 = x$, that of the

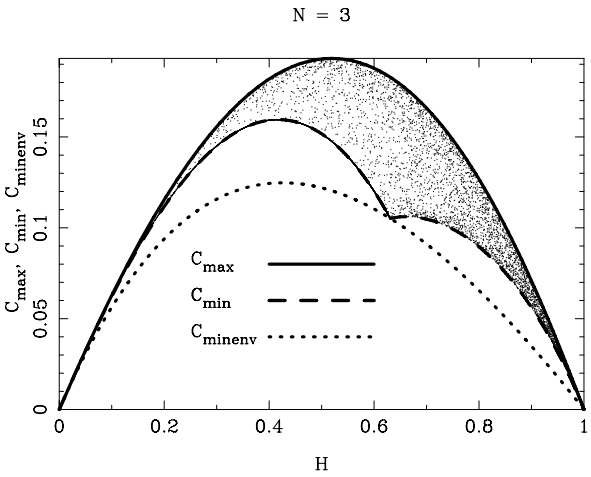

Fig. 4.2 In general, dependence of complexity (C) on normalized information (H) is not univocal: many distributions $\{p_i\}$ can present the same value of H but different C. This is shown in the case $N = 3$

second one is simply $p_2 = 1 - x$. The complexity of the system will be:

$$C(x) = H(x) \cdot D(x)$$
$$= -\frac{1}{\log 2}\left[x \log\left(\frac{x}{1-x}\right) + \log(1-x)\right] \cdot 2\left(x - \frac{1}{2}\right)^2 . \qquad (4.5)$$

Complexity vanishes for the two simplest 2-systems: the crystal ($H = 0$; $p_1 = 1$, $p_2 = 0$) and the ideal gas ($H = 1$; $p_1 = 1/2$, $p_2 = 1/2$). Let us notice that this curve is the simplest one that fulfills all the conditions discussed in the introduction. The largest complexity is reached for $H \sim 1/2$ and its value is: $C(x \sim 0.11) \sim 0.151$. For $N > 2$ the relationship between H and C is not univocal anymore. Many different distributions $\{p_i\}$ store the same information H but have different complexity C. Figure 4.2 displays such a behavior for $N = 3$. If we take the maximum complexity $C_{\max}(H)$ associated with each H a curve similar to the one for a 2-system is recovered. Every 3-system will have a complexity below this line and upper the line of $C_{\min}(H)$ and also upper the minimum envelope complexity C_{minenv}. These lines will be analytically found in a next section. In Fig. 4.3 curves $C_{\max}(H)$ for the cases $N = 3, \ldots, 10$ are also shown. Let us observe the shift of the complexity-curve peak to smaller values of entropy for rising N. This fact agrees with the intuition telling us that the biggest complexity (number of possibilities of 'complexification') be reached for lesser entropies for the systems with bigger number of states.

Let us return to the point at which we started this discussion. Any notion of complexity in physics [2, 3] should only be made on the basis of a well defined or operational magnitude [6, 7]. But two additional requirements are needed in order to obtain a good definition of complexity in physics: (1) the new magnitude must be measurable in many different physical systems and (2) a comparative relationship and a physical interpretation between any two measurements should be possible.

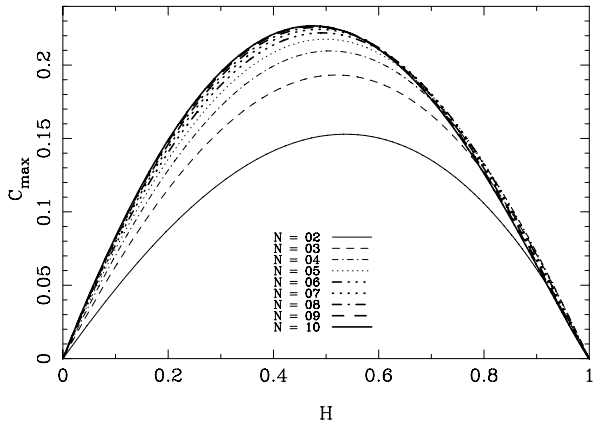

Fig. 4.3 Complexity ($C = H \cdot D$) as a function of the normalized information (H) for a system with two accessible states ($N = 2$). Also curves of maximum complexity ($C_{\max}$) are shown for the cases: $N = 3, \ldots, 10$

Many different definitions of complexity have been proposed to date, mainly in the realm of physical and computational sciences. Among these, several can be cited: algorithmic complexity (Kolmogorov-Chaitin) [8–10], the Lempel-Ziv complexity [11], the logical depth of Bennett [12], the effective measure complexity of Grassberger [13], the complexity of a system based in its diversity [14], the thermodynamical depth [15], the ε-machine complexity [16], the physical complexity of genomes [17], complexities of formal grammars, etc. The definition of complexity (4.3) proposed in this section offers a new point of view, based on a statistical description of systems at a given *scale*. In this scheme, the knowledge of the physical laws governing the dynamic evolution in that scale is used to find its accessible states and its probability distribution. This process would immediately indicate the value of complexity. In essence this is nothing but an interplay between the information stored by the system and the *distance from equipartition* (measure of a probabilistic hierarchy between the observed parts) of the probability distribution of its accessible states. Besides giving the main features of a "intuitive" notion of complexity, we will show in this chapter that we can go one step further and to compute this quantity in other relevant physical situations and in continuum systems. The most important point is that the new definition successfully enables us to discern situations regarded as complex. For example, we show here two of these applications in complex systems with some type of discretization: one of them is the study of this magnitude in a phase transition in a coupled map lattice [18] and the other one is its calculation for the time evolution of a discrete gas out of equilibrium [19]. Other applications to more realistic systems can also be found in the literature [20].

4.1.1 Complexity in a Phase Transition: Coupled Map Lattices

If by complexity it is to be understood that property present in all systems attached under the epigraph of 'complex systems', this property should be reasonably quantified by the measures proposed in the different branches of knowledge. As discussed above, this kind of indicators is found in those fields where the concept of information is crucial, from physics [13, 15] to computational sciences [8–11, 16].

In particular, taking into account the statistical properties of a system, the indicator called the *LMC* (*LópezRuiz-Mancini-Calbet*) *complexity* has been introduced [6, 7] in the former section. This magnitude identifies the entropy or information H stored in a system and its disequilibrium D, i.e. the distance from its actual state to the probability distribution of equilibrium, as the two basic ingredients for calculating its complexity. Hence, the LMC complexity C is given by the formula (4.3), $C(\bar{p}) = H(\bar{p}) \cdot D(\bar{p})$, where $\bar{p} = \{p_i\}$, with $p_i > 0$ and $i = 1, \ldots, N$, represents the distribution of the N accessible states to the system, and k is a constant taken as $1/\log N$.

As well as the Euclidean distance D is present in the original LMC complexity, other kinds of disequilibrium measures have been proposed in order to remedy some statistical characteristics considered troublesome for some authors [21]. In particular, some attention has been focused [22, 23] on the Jensen-Shannon divergence D_{JS} as a measure for evaluating the distance between two different distributions $(\bar{p}_1, \bar{p}_2)$. This distance reads:

$$D_{JS}(\bar{p}_1, \bar{p}_2) = H(\pi_1 \bar{p}_1 + \pi_2 \bar{p}_2) - \pi_1 H(\bar{p}_1) - \pi_2 H(\bar{p}_2), \tag{4.6}$$

with π_1, π_2 the weights of the two probability distributions $(\bar{p}_1, \bar{p}_2)$ verifying $\pi_1, \pi_2 \geq 0$ and $\pi_1 + \pi_2 = 1$. The ensuing statistical complexity

$$C_{JS} = H \cdot D_{JS} \tag{4.7}$$

becomes intensive and also keeps the property of distinguishing among distinct degrees of periodicity [24]. In this section, we consider $\bar{p}_2$ the equiprobability distribution and $\pi_1 = \pi_2 = 0.5$.

As it can be straightforwardly seen, all these LMC-like complexities vanish both for completely ordered and for completely random systems as it is required for the correct asymptotic properties of a such well-behaved measure. Recently, they have been successfully used to discern situations regarded as complex in discrete systems out of equilibrium [19, 25–31].

Here, the local transition to chaos via intermittency [32] in the logistic map, $x_{n+1} = \lambda x_n (1 - x_n)$ presents a sharp transition when C is plotted versus the parameter λ in the region around the instability for $\lambda \sim \lambda_t = 3.8284$. When $\lambda < \lambda_t$ the system approaches the laminar regime and the bursts become more unpredictable. The complexity increases. When the point $\lambda = \lambda_t$ is reached a drop to zero occurs for the magnitude C. The system is now periodic and it has lost its complexity. The dynamical behavior of the system is finally well reflected in the magnitude C as it has been studied in [7].

When a one-dimensional array of such maps is put together a more complex behavior can be obtained depending on the coupling among the units. Ergo the phenomenon called *spatio-temporal intermittency* can emerge [33–35]. This dynamical regime corresponds with a situation where each unit is weakly oscillating around a laminar state that is aperiodically and strongly perturbed for a traveling burst. In this case, the plot of the one-dimensional lattice evolving in time gives rise to complex patterns on the plane. If the coupling among units is modified the system can settle down in an absorbing phase where its dynamics is trivial [36, 37] and then homogeneous patterns are obtained. Therefore an abrupt transition to spatio-temporal intermittency can be depicted by the system [38, 39] when modifying the coupling parameter.

Now we are concerned with measuring C and C_{JS} in a such transition for a coupled map lattice of logistic type. Our system will be a line of sites, $i = 1, \ldots, L$, with periodic boundary conditions. In each site i a local variable x_i^n evolves in time (n) according to a discrete logistic equation. The interaction with the nearest neighbors takes place via a multiplicative coupling:

$$x_i^{n+1} = (4 - 3pX_i^n)x_i^n(1 - x_i^n), \tag{4.8}$$

where p is the parameter of the system measuring the strength of the coupling $(0 < p < 1)$. The variable X_i^n is the digitalized local mean field,

$$X_i^n = \text{nint}\left[\frac{1}{2}(x_{i+1}^n + x_{i-1}^n)\right], \tag{4.9}$$

with nint(.) the integer function rounding its argument to the nearest integer. Hence $X_i^n = 0$ or 1.

There is a biological motivation behind this kind of systems [40, 41]. It could represent a *colony of interacting competitive individuals*. They evolve randomly when they are independent ($p = 0$). If some competitive interaction ($p > 0$) among them takes place the local dynamics loses its erratic component and becomes chaotic or periodic in time depending on how populated the vicinity is. Hence, for bigger X_i^n more populated is the neighborhood of the individual i and more constrained is its free action. At a first sight, it would seem that some particular values of p could stabilize the system. In fact, this is the case. Let us choose a number of individuals for the colony ($L = 500$ for instance), let us initialize it randomly in the range $0 < x_i < 1$ and let it evolve until the asymptotic regime is attained. Then the *black/white* statistics of the system is performed. That is, the state of the variable x_i is compared with the critical level 0.5 for $i = 1, \ldots, L$: if $x_i > 0.5$ the site i is considered *white* (high density cell) and a counter N_w is increased by one, or if $x_i < 0.5$ the site i is considered *black* (low density cell) and a counter N_b is increased by one. This process is executed in the stationary regime for a set of iterations. The *black/white* statistics is then the rate $\beta = N_b/N_w$. If β is plotted versus the coupling parameter p Fig. 4.4 is obtained.

The region $0.258 < p < 0.335$ where β vanishes is remarkable. As stated above, β represents the rate between the number of black cells and the number of white

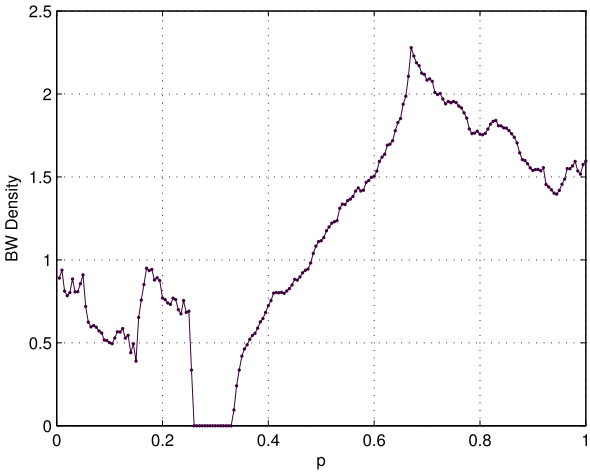

Fig. 4.4 β versus p. The β-statistics (or BW density) for each p is the rate between the number of *black* and *white* cells depicted by the system in the two-dimensional representation of its after-transient time evolution. (Computations have been performed with $\Delta p = 0.005$ for a lattice of 10000 sites after a transient of 5000 iterations and a running of other 2000 iterations)

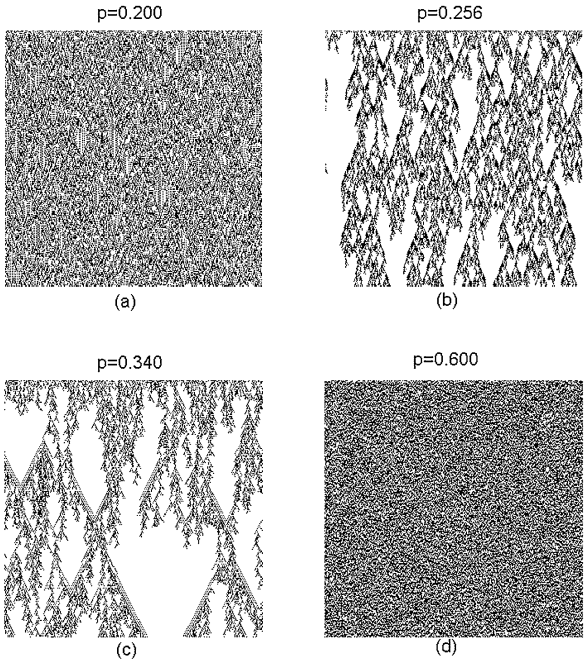

Fig. 4.5 Digitalized plot of the one-dimensional coupled map lattice (axe OX) evolving in time (axe OY) according to (4.8): if $x_i^n > 0.5$ the (i, n)-cell is put in *white color* and if $x_i^n < 0.5$ the (i, n)-cell is put in *black color*. The discrete time n is reset to zero after the transitory. (Lattices of 300×300 sites, i.e., $0 < i < 300$ and $0 < n < 300$)

cells appearing in the two-dimensional digitalized representation of the colony evolution. A whole white pattern is obtained for this range of p. The phenomenon of spatio-temporal intermittency is displayed by the system in the two borders of this parameter region (Fig. 4.5). Bursts of low density (black color) travel in an irregular way through the high density regions (white color). In this case two-dimensional complex patterns are shown by the time evolution of the system (Fig. 4.5b–c). If the coupling p is far enough from this region, i.e., $p < 0.25$ or $p > 0.4$, the absorbent

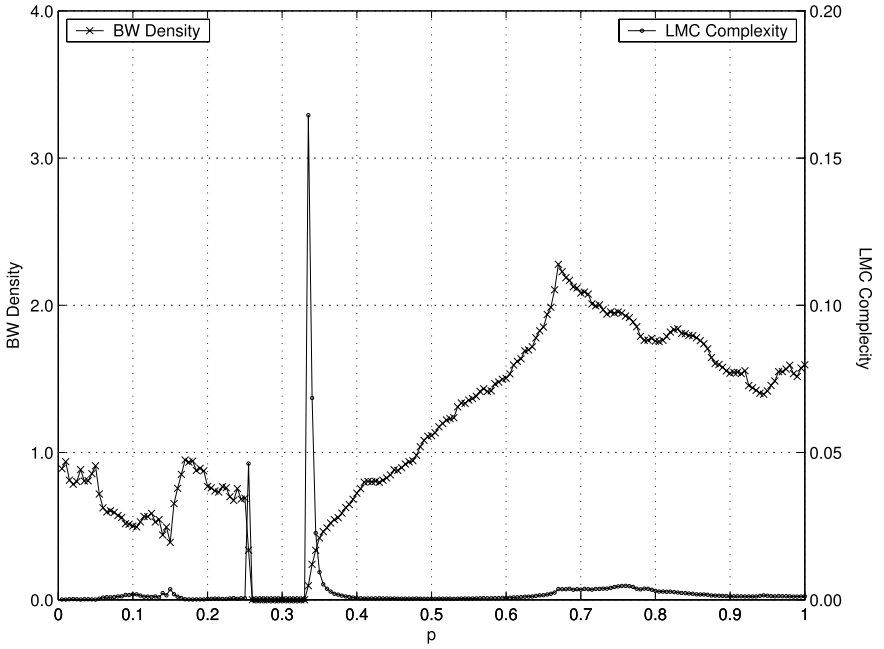

Fig. 4.6 (•) C versus p. Observe the peaks of the LMC complexity located just on the borders of the absorbent region $0.258 < p < 0.335$, where $\beta = 0$ ($\times$). (Computations have been performed with $\Delta p = 0.005$ for a lattice of 10000 sites after a transient of 5000 iterations and a running of other 2000 iterations)

region loses its influence on the global dynamics and less structured and more random patterns than before are obtained (Fig. 4.5a–d). For $p = 0$ we have no coupling of the maps, and each map generates so called fully developed chaos, where the invariant measure is well-known to be symmetric around 0.5. From this we conclude that $\beta(p = 0) = 1$. Let us observe that this symmetrical behavior of the invariant measure is broken for small p, and β decreases slightly in the vicinity of $p = 0$.

If the LMC complexities are quantified as function of p, our *intuition* is confirmed. The method proposed in [7] to calculate C is now adapted to the case of two-dimensional patterns. First, we let the system evolve until the asymptotic regime is attained. This transient is discarded. Then, for each time n, we map the whole lattice in a binary sequence: 0 if $x_i^n < 0.5$ and 1 if $x_i^n > 0.5$, for $i = 1, \ldots, L$. This L-binary string is analyzed by blocks of n_o bits, where n_o can be considered the scale of observation. For this scale, there are 2^{n_o} possible states but only some of them are accessible. These accessible states as well as their probabilities are found in the L-binary string. Next, the magnitudes H, D, D_{JS}, C and C_{JS} are directly calculated for this particular time n by applying the formulas (4.3), (4.7). We repeat this process for a set of successive time units $(n, n+1, \ldots, n+m)$. The mean values of H, D, D_{JS}, C and C_{JS} for these m time units are finally obtained and plotted in Figs. 4.6, 4.7.

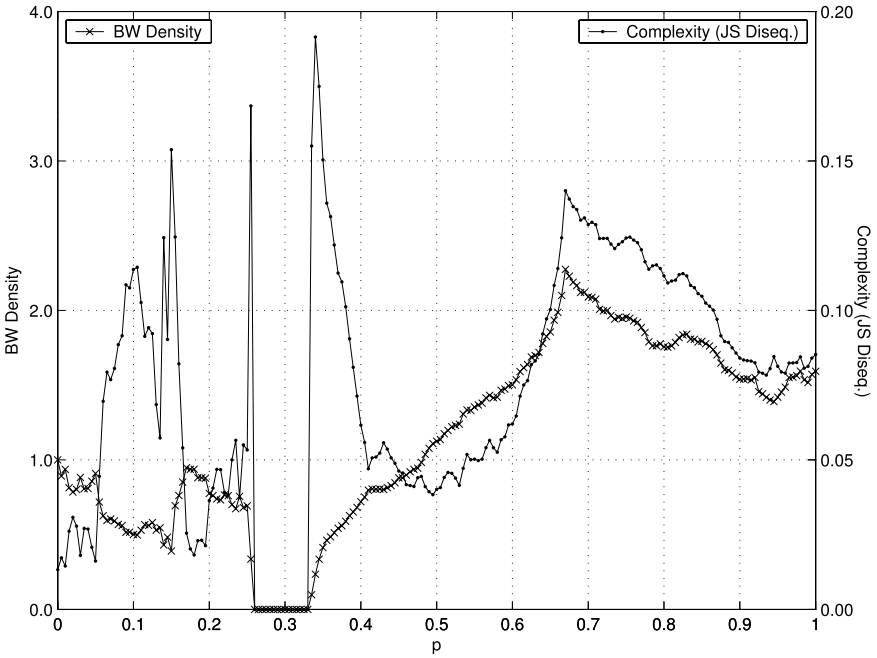

Fig. 4.7 $(\cdot)\, C_{JS}$ versus p. The peaks of this modified LMC complexity are also evident just on the borders of the absorbent region $0.258 < p < 0.335$, where $\beta = 0$ $(\times)$. (Computations have been performed with $\Delta p = 0.005$ for a lattice of 10000 sites after a transient of 5000 iterations and a running of other 2000 iterations)

Figures 4.6, 4.7 show the result for the case of $n_o = 10$. Let us observe that the highest C and C_{JS} are reached when the dynamics displays spatio-temporal intermittency, that is, the *most complex patterns* are obtained for those values of p that are located on the borders of the absorbent region $0.258 < p < 0.335$. Thus the plot of C and C_{JS} versus p shows two tight peaks around the values $p = 0.256$ and $p = 0.34$ (Figs. 4.6, 4.7). Let us remark that the LMC complexity C can be neglected far from the absorbent region. Contrarily to this behavior, the magnitude C_{JS} also shows high peaks in some other sharp transition of β located in the region $0 < p < 25$, and an intriguing correlation with the *black/white* statistics in the region $0.4 < p < 1$. All these facts as well as the stability study of the different dynamical regions of system (4.8) are not the object of the present writing but they could deserve some attention in a further inspection.

If the detection of complexity in the two-dimensional case requires to identify some sharp change when comparing different patterns, those regions in the parameter space where an abrupt transition happens should be explored in order to obtain the most complex patterns. Smoothness seems not to be at the origin of complexity. As well as a selected few distinct molecules among all the possible are in the basis of life [42], discreteness and its spiky appearance could indicate the way towards

complexity. As we show in the next section, the distributions with the highest LMC complexity are just those distributions with a spiky-like appearance [19]. In this line, the striking result here exposed confirms the capability of the LMC-like complexities for signaling a transition to complex behavior when regarding two-dimensional patterns [18, 43].

4.1.2 Complexity Versus Time: The Tetrahedral Gas

As before explained, several definitions of complexity, in the general sense of the term, have been presented in the literature. These can be classified according to their calculation procedure into two broad and loosely defined groups. One of these groups is based on computational science and consists of all definitions based on algorithms or automata to derive the complexity. Examples are the algorithmic complexity [9, 10], the logical depth [12] and the ε-machine complexity [16]. These definitions have been shown to be very useful in describing symbolic dynamics of chaotic maps, but they have the disadvantage of being very difficult to calculate. Another broad group consists of those complexities based on the measure of entropy or entropy rate. Among these, we may cite the effective measure complexity [13], the thermodynamic depth [15], the simple measure for complexity [26] and the metric or K–S entropy rate [44, 45]. These definitions have also been very useful in describing symbolic dynamics in maps, the simple measure of complexity having been also applied to some physical situation such as a non-equilibrium Fermi gas [46]. They suffer the disadvantage of either being very difficult to calculate or having a simple relation to the regular entropy.

Other definition types of complexity have been introduced. These are based on quantities that can be calculated directly from the distribution function describing the system. One of these is based on "meta-statistics" [47] and the other on the notion of "disequilibrium" [7]. This latter definition has been referred above as the LMC complexity. These definitions, together with the simple measure for complexity [26], have the great advantage of allowing easy calculations within the context of kinetic theory and of permitting their evaluation in a natural way in terms of statistical mechanics.

As we have shown in the former sections, the disequilibrium-based complexity is easy to calculate and shows some interesting properties [7], but suffers from the main drawback of not being very well behaved as the system size increases, or equivalently, as the distribution function becomes continuous. Feldman and Crutchfield [21] tried to solve this problem by defining another equivalent term for disequilibrium, but ended up with a complexity that was a trivial function of the entropy.

Whether these definitions of complexity are useful in non-equilibrium thermodynamics will depend on how they behave as a function of time. There is a general

belief that, although the second law of thermodynamics requires average entropy (or disorder) to increase, this does not in any way forbid local order from arising [48]. The clearest example is seen with life, which can continue to exist and grow in an isolated system for as long as internal resources last. In other words, in an isolated system the entropy must increase, but it should be possible, under certain circumstances, for the complexity to increase.

Here we examine how LMC complexity evolves with time in an isolated system and we show that it indeed has some interesting properties. The disequilibrium-based complexity [7] defined in (4.3) actually tends to be maximal as the entropy increases in a Boltzmann integro-differential equation for a simplified gas.

We proceed to calculate the distributions which maximize and minimize the complexity and its asymptotic behavior, and also introduce the basic concepts underlying the time evolution of LMC complexity in Sect. 4.1.2.1. Later, in Sects. 4.1.2.2 and 4.1.2.3, by means of numerical computations following a restricted version of the Boltzmann equation, we apply this to a special system, which we shall term "tetrahedral gas". Finally, in Sect. 4.1.2.4, the results and conclusions for this system are given, together with their possible applications.

4.1.2.1 Maximum and Minimum Complexity

In this section, we assume that the system can be in one of its N possible accessible states, i. The probability of the system being in state i will be given by the discrete distribution function, $f_i \geq 0$, with the normalization condition $I \equiv \sum_{i=1}^{N} f_i = 1$. The system is defined such that, if isolated, it will reach equilibrium, with all the states having equal probability, $f_e = \frac{1}{N}$. Since we are supposing that H is normalized, $0 \leq H \leq 1$, and $0 \leq D \leq (N-1)/N$, then complexity, C, is also normalized, $0 \leq C \leq 1$.

When an isolated system evolves with time, the complexity cannot have any possible value in a C versus H map as it can be seen in Fig. 4.2, but it must stay within certain bounds, $C_{\max}$ and $C_{\min}$. These are the maximum and minimum values of C for a given H. Since $C = D \cdot H$, finding the extrema of C for constant H is equivalent to finding the extrema of D.

There are two restrictions on D: the normalization, I, and the fixed value of the entropy, H. To find these extrema undetermined Lagrange multipliers are used. Differentiating expressions of D, I and H, we obtain

$$\frac{\partial D}{\partial f_j} = 2(f_j - f_e), \tag{4.10}$$

$$\frac{\partial I}{\partial f_j} = 1, \tag{4.11}$$

$$\frac{\partial H}{\partial f_j} = -\frac{1}{\ln N}(\ln f_j + 1). \tag{4.12}$$

Table 4.1 Probability values, f_j, that give a maximum of disequilibrium, $D_{\max}$, for a given H

Number of states with f_j	f_j	Range of f_j
1	$f_{\max}$	$\frac{1}{N} \ldots 1$
$N-1$	$\frac{1-f_{\max}}{N-1}$	$0 \ldots \frac{1}{N}$

Table 4.2 Probability values, f_j, that give a minimum of disequilibrium, $D_{\min}$, for a given H

n can have the values $0, 1, \ldots, N-2$

Number of states with f_j	f_j	Range of f_j
n	0	0
1	$f_{\min}$	$0 \ldots \frac{1}{N-n}$
$N-n-1$	$\frac{1-f_{\min}}{N-n-1}$	$\frac{1}{N-n} \cdots \frac{1}{N-n-1}$

Defining λ_1 and λ_2 as the Lagrange multipliers, we get:

$$2(f_j - f_e) + \lambda_1 + \lambda_2(\ln f_j + 1)/\ln N = 0. \tag{4.13}$$

Two new parameters, α and β, which are a linear combinations of the Lagrange multipliers are defined:

$$f_j + \alpha \ln f_j + \beta = 0, \tag{4.14}$$

where the solutions of this equation, f_j, are the values that minimize or maximize the disequilibrium.

In the maximum complexity case there are two solutions, f_j, to (4.14) which are shown in Table 4.1. One of these solutions, $f_{\max}$, is given by

$$H = -\frac{1}{\ln N}\left[f_{\max} \ln f_{\max} + (1 - f_{\max}) \ln\left(\frac{1 - f_{\max}}{N-1}\right)\right], \tag{4.15}$$

and the other solution by $(1 - f_{\max})/(N-1)$.

The maximum disequilibrium, $D_{\max}$, for a fixed H is

$$D_{\max} = (f_{\max} - f_e)^2 + (N-1)\left(\frac{1 - f_{\max}}{N-1} - f_e\right)^2, \tag{4.16}$$

and thus, the maximum complexity, which depends only on H, is

$$C_{\max}(H) = D_{\max} \cdot H. \tag{4.17}$$

The behavior of the maximum value of complexity versus $\ln N$ was computed in [49].

Equivalently, the values, f_j, that give a minimum complexity are shown in Table 4.2. One of the solutions, $f_{\min}$, is given by

$$H = -\frac{1}{\ln N}\left[f_{\min} \ln f_{\min} + (1 - f_{\min}) \ln\left(\frac{1 - f_{\min}}{N-n-1}\right)\right], \tag{4.18}$$

where n is the number of states with $f_j = 0$ and takes a value in the range $n = 0, 1, \ldots, N-2$.

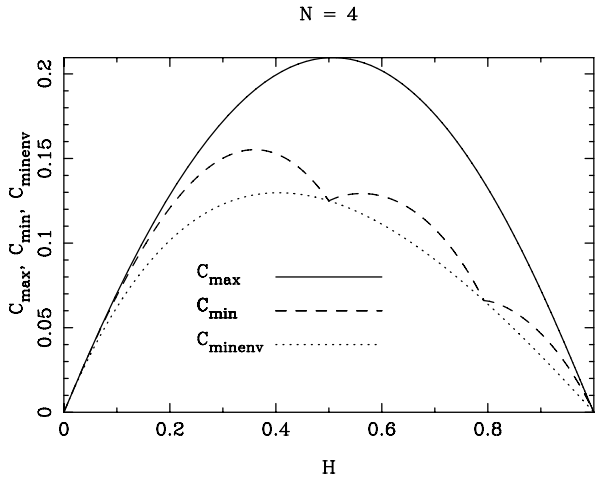

Fig. 4.8 Maximum, minimum, and minimum envelope complexity, $C_{\max}$, $C_{\min}$, and C_{minenv} respectively, as a function of the entropy, H, for a system with $N = 4$ accessible states

The resulting minimum disequilibrium, $D_{\min}$, for a given H is,

$$D_{\min} = (f_{\min} - f_e)^2 + (N - n - 1)\left(\frac{1 - f_{\min}}{N - n - 1} - f_e\right)^2 + n f_e^2. \tag{4.19}$$

Note that in this case $f_j = 0$ is an additional hidden solution that stems from the positive restriction in the f_i values. To obtain these solutions explicitly we can define x_i such that $f_i \equiv {x_i}^2$. These x_i values do not have the restriction of positivity imposed to f_i and can take a positive or negative value. If we repeat the Lagrange multiplier method with these new variables a new solution arises: $x_j = 0$, or equivalently, $f_j = 0$.

The resulting minimum complexity, which again only depends on H, is

$$C_{\min}(H) = D_{\min} \cdot H. \tag{4.20}$$

As an example, the maximum and minimum of complexity, $C_{\max}$ and $C_{\min}$, are plotted as a function of the entropy, H, in Fig. 4.8 for $N = 4$. Also, in this figure, it is shown the minimum envelope complexity, $C_{\text{minenv}} = D_{\text{minenv}} \cdot H$, where D_{minenv} is defined below. In Fig. 4.9 the maximum and minimum disequilibrium, $D_{\max}$ and $D_{\min}$, versus H are also shown.

As shown in Fig. 4.9 the minimum disequilibrium function is piecewise defined, having several points where its derivative is discontinuous. Each of these function pieces corresponds to a different value of n (Table 4.2). In some circumstances it might be helpful to work with the "envelope" of the minimum disequilibrium function. The function, D_{minenv}, that traverses all the discontinuous derivative points in the $D_{\min}$ versus H plot is

$$D_{\text{minenv}} = e^{-H \ln N} - \frac{1}{N}, \tag{4.21}$$

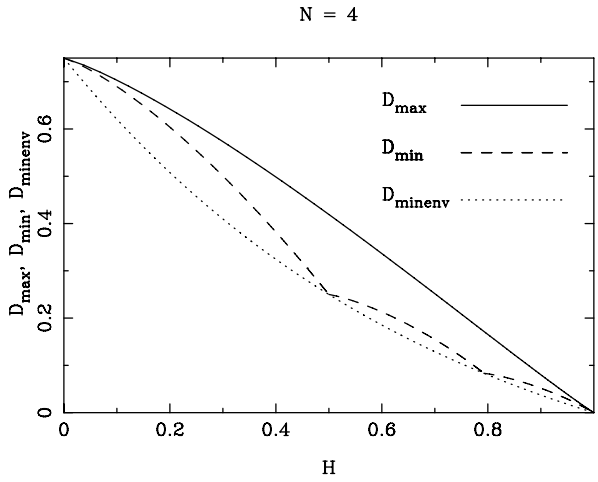

Fig. 4.9 Maximum, minimum, and minimum envelope disequilibrium, $D_{\max}$, $D_{\min}$, and D_{minenv} respectively, as a function of the entropy, H, for a system with $N = 4$ accessible states

and is also shown in Fig. 4.9.

When N tends toward infinity the probability, $f_{\max}$, of the dominant state has a linear dependence with the entropy,

$$\lim_{N\to\infty} f_{\max} = 1 - H, \tag{4.22}$$

and thus the maximum disequilibrium scales as $\lim_{N\to\infty} D_{\max} = (1 - H)^2$. The maximum complexity tends to

$$\lim_{N\to\infty} C_{\max} = H \cdot (1 - H)^2 . \tag{4.23}$$

The limit of the minimum disequilibrium and complexity vanishes, $\lim_{N\to\infty} D_{\text{minenv}} = 0$, and thus

$$\lim_{N\to\infty} C_{\min} = 0. \tag{4.24}$$

In general, in the limit $N \to \infty$, the complexity is not a trivial function of the entropy, in the sense that for a given H there exists a range of complexities between 0 and $C_{\max}$, given by (4.24) and (4.23), respectively.

In particular, in this asymptotic limit, the maximum of $C_{\max}$ is found when $H = 1/3$, or equivalently $f_{\max} = 2/3$, which gives a maximum of the maximum complexity of $C_{\max} = 4/27$. This value was numerically calculated in [49].

4.1.2.2 An out Equilibrium System: The Tetrahedral Gas

We present a simplified example of an ideal gas: the tetrahedral gas. This system is generated by a simplification of the Boltzmann integro-differential equation of an ideal gas. We are interested in studying the disequilibrium time evolution.

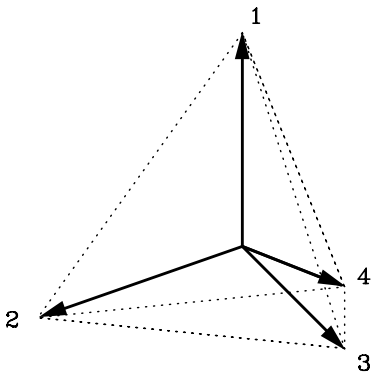

Fig. 4.10 The four possible directions of the velocities of the tetrahedral gas in space. Positive senses are defined as emerging from the center point and with integer numbers 1, 2, 3, 4

The Boltzmann integro-differential equation of an ideal gas with no external forces and no spatial gradients is

$$\frac{\partial f(\mathbf{v};t)}{\partial t} = \int d^3\mathbf{v}_* \int d\Omega_{\text{c.m.}} \sigma(\mathbf{v}_* - \mathbf{v} \to \mathbf{v}'_* - \mathbf{v}')|\mathbf{v}_* - \mathbf{v}| \times \left[f(\mathbf{v}'_*;t) f(\mathbf{v}';t) - f(\mathbf{v}_*;t) f(\mathbf{v};t) \right], \tag{4.25}$$

where σ represents the cross section of a collision between two particles with initial velocities $\mathbf{v}$ and $\mathbf{v}_*$ and after the collision with velocities $\mathbf{v}'$ and $\mathbf{v}'_*$; and $\Omega_{\text{c.m.}}$ are all the possible dispersion angles of the collision as seen from its center of mass.

In the tetrahedral gas, the particles can travel only in four directions in three-dimensional space and all have the same absolute velocity. These directions are the ones given by joining the center of a tetrahedron with its corners. The directions can be easily viewed by recalling the directions given by a methane molecule, or equivalently, by a caltrop, which is a device with four metal points so arranged that when any three are on the ground the fourth projects upward as a hazard to the hooves of horses or to pneumatic tires (see Fig. 4.10).

By definition, the angle that one direction forms with any other is the same. It can be shown that the angles between different directions, α, satisfy the relationship $\cos\alpha = -1/3$, which gives $\alpha = 109.47°$. The plane formed by any two directions is perpendicular to the plane formed by the remaining two directions.

We assume that the cross-section, σ, is different from zero only when the angle between the velocities of the colliding particles is 109.47°. It is also assumed that this collision makes the two particles leave in the remaining two directions, thus again forming an angle of 109.47°. A consequence of these restrictions is that the modulus of the velocity is always the same no matter how many collisions a particle has undergone and they always stay within the directions of the vertices of the tetrahedron. Furthermore, this type of gas does not break any law of physics and is perfectly valid, although hypothetical.

We label the four directions originating from the center of the caltrop with numbers, **1**, **2**, **3**, **4** (see Fig. 4.10). The velocity components with the same direction but

Table 4.3 Cross sections, σ, for a particle in direction $-\mathbf{1}$ colliding with particles in the other remaining directions of the tetrahedral gas

Collision of particles	Cross section σ
$(-\mathbf{1}, -\mathbf{2}) \to (\mathbf{3}, \mathbf{4})$	1
$(-\mathbf{1}, -\mathbf{3}) \to (\mathbf{2}, \mathbf{4})$	1
$(-\mathbf{1}, -\mathbf{4}) \to (\mathbf{2}, \mathbf{3})$	1
Other collisions	0

opposite sense, or equivalently, directed toward the center of the caltrop, are labeled with negative numbers $-\mathbf{1}$, $-\mathbf{2}$, $-\mathbf{3}$, $-\mathbf{4}$.

In order to formulate the Boltzmann equation for the tetrahedral gas, and because all directions are equivalent, we need only study the different collisions that a particle with one fixed direction can undergo. In particular if we take a particle with direction $-\mathbf{1}$ the result of the collision with another particle with direction $-\mathbf{2}$ are the same two particles traveling in directions $\mathbf{3}$ and $\mathbf{4}$, that is,

$$(-\mathbf{1}, -\mathbf{2}) \to (\mathbf{3}, \mathbf{4}). \tag{4.26}$$

With this in mind the last bracket of (4.25) is,

$$f_3 f_4 - f_{-1} f_{-2}, \tag{4.27}$$

where f_i denotes the probability of finding a particle in direction $\mathbf{i}$. Note that the dependence on velocity, $\mathbf{v}$, of the continuous velocity distribution function, $f(\mathbf{v}; t)$, of (4.25) is in our case contained in the discrete subindex, i, of the distribution function f_i.

We can proceed in the same manner with the other remaining collisions,

$$\begin{aligned} (-\mathbf{1}, -\mathbf{3}) &\to (\mathbf{2}, \mathbf{4}), \\ (-\mathbf{1}, -\mathbf{4}) &\to (\mathbf{2}, \mathbf{3}). \end{aligned} \tag{4.28}$$

When a particle with direction $-\mathbf{1}$ collides with a particle with direction $\mathbf{2}$, they do not form an angle of 109.47°; i.e., they do not collide, they just pass by each other. This is a consequence of the previous assumption for the tetrahedral gas, which establishes a null cross section for angles different from 109.47°. The same can be said for collisions $(-\mathbf{1}, \mathbf{3})$, $(-\mathbf{1}, \mathbf{4})$, and $(-\mathbf{1}, \mathbf{1})$. All these results are summarized in Table 4.3.

Taking all this into account, (4.25) for direction $-\mathbf{1}$ is reduced to a discrete sum,

$$\frac{df_{-1}}{dt} = (f_3 f_4 - f_{-1} f_{-2}) + (f_2 f_4 - f_{-1} f_{-3}) + (f_2 f_3 - f_{-1} f_{-4}), \tag{4.29}$$

where all other factors have been set to unity for simplicity.

The seven remaining equations for the rest of directions can be easily inferred. If we now make $f_i = f_{-i}$ $(i = 1, 2, 3, 4)$ initially, this property is conserved in time. The final four equations defining the evolution of the system are:

$$\begin{aligned}
\frac{df_1}{dt} &= (f_3 f_4 - f_1 f_2) + (f_2 f_4 - f_1 f_3) + (f_2 f_3 - f_1 f_4), \\
\frac{df_2}{dt} &= (f_3 f_4 - f_1 f_2) + (f_1 f_4 - f_2 f_3) + (f_1 f_3 - f_2 f_4), \\
\frac{df_3}{dt} &= (f_2 f_4 - f_3 f_1) + (f_1 f_4 - f_3 f_2) + (f_1 f_2 - f_3 f_4), \\
\frac{df_4}{dt} &= (f_2 f_3 - f_4 f_1) + (f_1 f_3 - f_4 f_2) + (f_1 f_2 - f_3 f_4).
\end{aligned} \tag{4.30}$$

Note that the ideal gas has been reduced to the tetrahedral gas, which is a four-dimensional dynamical system. The velocity distribution function, f_i, corresponds to a probability distribution function with $N = 4$ accessible states that evolve in time.

4.1.2.3 Evolution of the Tetrahedral Gas with Time

To study the time evolution of the complexity, a diagram of C versus time, t, can be used. But, as we know, the second law of thermodynamics states that the entropy grows monotonically with time, that is,

$$\frac{dH}{dt} \geq 0. \tag{4.31}$$

This implies that an equivalent way to study the time evolution of the complexity can be obtained by plotting C versus H. In this way, the entropy substitutes the time axis, since the former increases monotonically with the latter. The conversion from C vs. H to C vs. t diagrams is achieved by stretching or shrinking the entropy axis according to its time evolution. This method is a key point in all this discussion. Note that, in any case, the relationship of H versus t will, in general, not be a simple one [50].

The tetrahedral gas, (4.30), reaches equilibrium when $f_i = 1/N$ for $i = 1, 2, 3, 4$ and $N = 4$. This stationary state, $df_i/dt = 0$, represents the equiprobability towards which the system evolves in time. This is consistent with the definition of disequilibrium in which we assumed that equilibrium was reached at equiprobability, $f_i = f_e$, where $D = 0$.

As the isolated system evolves it gets closer and closer to equilibrium. In this sense, one may intuitively think that the disequilibrium will decrease with time. In fact, it can be analytically shown [19] that, as the system approaches to equilibrium, D tends to zero monotonically with time:

$$\frac{dD}{dt} \leq 0. \tag{4.32}$$

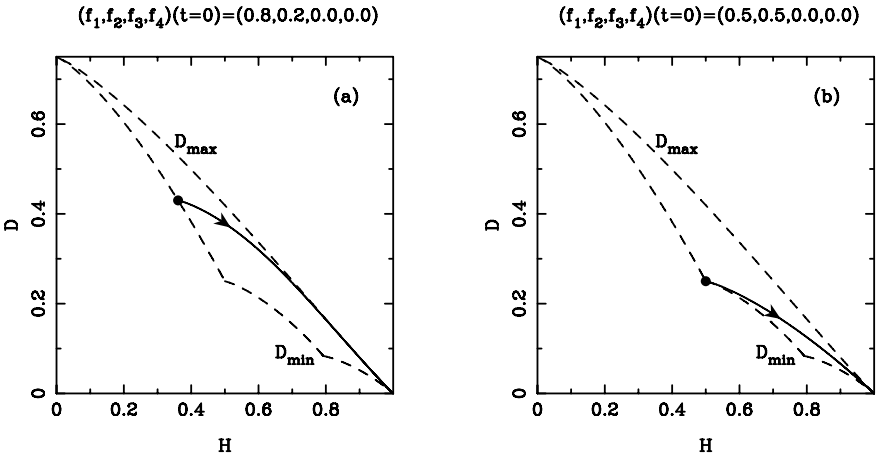

Fig. 4.11 Time evolution of the system in (H, D) phase space for two different initial conditions at time $t = 0$: (**a**) $(f_1, f_2, f_3, f_4) = (0.8, 0.2, 0, 0)$ and (**b**) $(f_1, f_2, f_3, f_4) = (0.5, 0.5, 0, 0)$. The maximum and minimum disequilibrium are shown by *dashed lines*

There are even more restrictions on the evolution of this system. It would be expected that the system approaches equilibrium, $D = 0$, by following the most direct path. To verify this, numerical simulations for several initial conditions have been undertaken. In all of these we observe the additional restriction that D approaches $D_{\max}$ on its way to $D = 0$. In fact it appears as an exponential decay of D towards $D_{\max}$ in a D versus H plot. As an example, two of these are shown in Fig. 4.11, where Fig. 4.11(a) shows a really strong tendency towards $D_{\max}$. Contrary to intuition, among all the possible paths that the system can follow toward equilibrium, it chooses those closest to $D_{\max}$ in particular.

We can also observe this effect in a complexity, C, versus H plot. This is shown for the same two initial conditions in Fig. 4.12.

This additional restriction to the evolution of the system is better viewed by plotting the difference $C_{\max} - C$ versus H. In all the cases analyzed (see two of them in Fig. 4.13) the following condition is observed:

$$\frac{d(C_{\max} - C)}{dt} \leq 0. \tag{4.33}$$

This has been verified numerically and is illustrated in Fig. 4.14, where this time derivative, which always remains negative, is shown as a function of H for a grid of uniformly spaced distribution functions, (f_1, f_2, f_3, f_4), satisfying the normalization condition I. Two system trajectories are also shown for illustrative purposes. The numerical method used to plot this function is explained in [19].

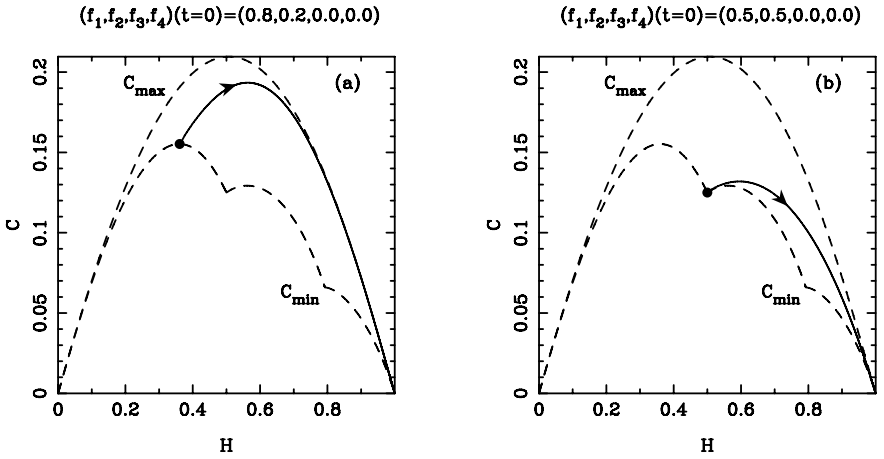

Fig. 4.12 Time evolution of the system in (H, C) phase space for two different initial conditions at time $t = 0$: (**a**) $(f_1, f_2, f_3, f_4) = (0.8, 0.2, 0, 0)$ and (**b**) $(f_1, f_2, f_3, f_4) = (0.5, 0.5, 0, 0)$. The maximum and minimum complexity are shown by *dashed lines*

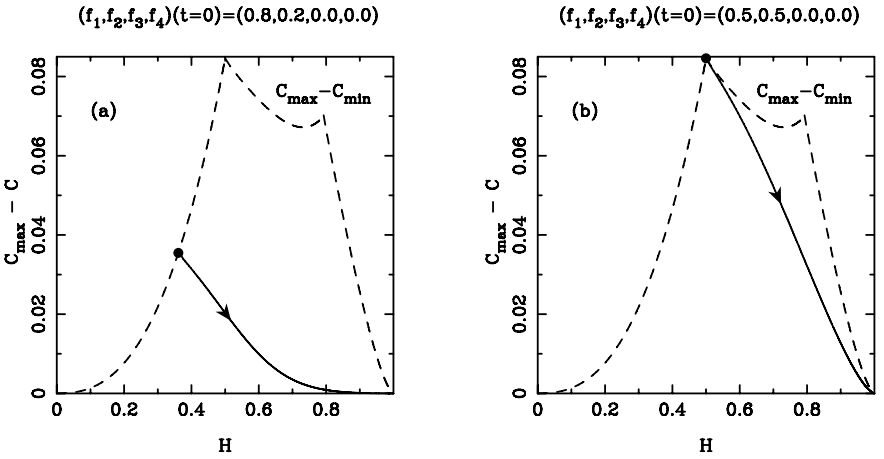

Fig. 4.13 Time evolution of the system in $(H, C_{\max} - C)$ phase space for two different initial conditions at time $t = 0$: (**a**) $(f_1, f_2, f_3, f_4) = (0.8, 0.2, 0, 0)$ and (**b**) $(f_1, f_2, f_3, f_4) = (0.5, 0.5, 0, 0)$. The values $C_{\max} - C_{\min}$ are shown by *dashed lines*

We proceed now to show another interesting property of this system. As shown in Table 4.1, a collection of maximum complexity distributions for $N = 4$ can take the form

$$\begin{aligned} f_1 &= f_{\max}, \\ f_i &= \frac{1 - f_{\max}}{3}, \quad i = 2, 3, 4, \end{aligned} \tag{4.34}$$

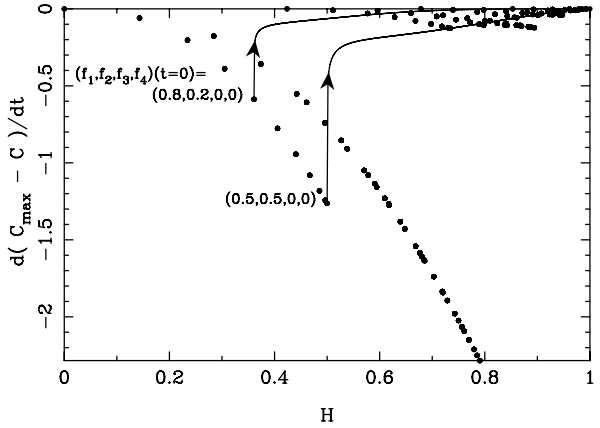

Fig. 4.14 Numerical verification of $d(C_{\max} - C)/dt \leq 0$. This time derivative is shown as a function of H. A grid of uniformly spaced, $\Delta f_i = 0.5$, distribution functions, (f_1, f_2, f_3, f_4), satisfying the normalization condition I, have been used. Two system trajectories for initial conditions, $t = 0$, $(f_1, f_2, f_3, f_4) = (0.8, 0.2, 0, 0)$ and $(f_1, f_2, f_3, f_4) = (0.5, 0.5, 0, 0)$ are also shown for illustrative purposes. It can be seen how the above-mentioned time derivative always remains negative

where $f_{\max}$ runs from $1/N$ (equiprobability distribution) to 1 ("crystal" distribution). The complexity of this collection of distributions covers all possible values of $C_{\max}$.

There is actually a time evolution of the tetrahedral gas, or trajectory of the system, formed by this collection of distributions. Inserting (4.34) in the evolution (4.30), it is found that all equations are compatible with each other and the dynamical equations are reduced to the relation,

$$\frac{df_{\max}}{dt} = \frac{1}{3}(4f_{\max}^2 - 5f_{\max} + 1). \tag{4.35}$$

This trajectory is denoted as the *maximum complexity path*.

Note that the equiprobability or equilibrium, $f_{\max} = 1/4$, is a stable fixed point and the maximum disequilibrium "crystal" distribution, $f_{\max} = 1$, is an unstable fixed point. Thus the maximum complexity path is a heteroclinic connection between the "crystal" and equiprobability distributions.

The maximum complexity path is locally attractive. Let us assume, for instance, the following perturbed trajectory

$$\begin{aligned} f_1 &= f_{\max}, \\ f_2 &= \frac{1 - f_{\max}}{3}, \\ f_3 &= \frac{1 - f_{\max}}{3} + \delta, \\ f_4 &= \frac{1 - f_{\max}}{3} - \delta, \end{aligned} \tag{4.36}$$

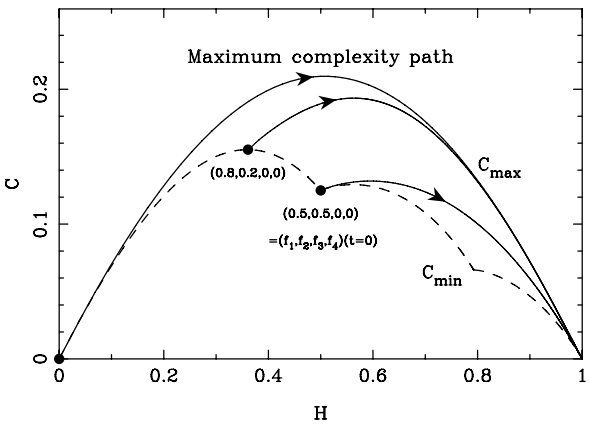

Fig. 4.15 The time evolution of the system for three different initial conditions, $t = 0$, $(f_1, f_2, f_3, f_4) = (0.8, 0.2, 0, 0)$, $(f_1, f_2, f_3, f_4) = (0.5, 0.5, 0, 0)$, and the maximum complexity path are shown. The minimum complexity is shown by *dashed lines*. It can be seen how the system tends to approach the maximum complexity path as it evolves in time toward equilibrium

whose evolution according to (4.30) gives the exponential decay of the perturbation, δ:

$$\frac{d\delta}{dt} \sim -\left(\frac{4f_{\max}+2}{3}\right)\delta, \tag{4.37}$$

showing the attractive nature of these trajectories.

4.1.2.4 Conclusions and Further Remarks

In the former section, the time evolution of the LMC complexity, C, has been studied for a simplified model of an isolated ideal gas: the tetrahedral gas. In general, the dynamical behavior of this quantity is bounded between two extremum curves, $C_{\max}$ and $C_{\min}$, when observed in a C versus H phase space. These complexity bounds have been derived and computed. A continuation of this work applied to the study of complexity in gases out of equilibrium can be found in [51, 52].

For the isolated tetrahedral gas two constraints on its dynamics are found. The first, which is analytically demonstrated, is that the disequilibrium, D, decreases monotonically with time until it reaches the value $D = 0$ for the equilibrium state. The second is that the maximum complexity paths, $C_{\max}$, are attractive in phase space. In other words, the complexity of the system tends to equilibrium always approaching those paths. This has been verified numerically, that is, the time derivative of the difference between $C_{\max}$ and C is negative. Figure 4.15 summarizes the dynamical behavior of the tetrahedral gas. The different trajectories starting with arbitrary initial conditions, which represent systems out of equilibrium, evolve towards equilibrium approaching the maximum complexity path.

Whether these properties are useful in real physical systems can need of a further inspection, particularly the macroscopical nature of the disequilibrium in more

general systems, such as to the ideal gas following the complete Boltzmann integro–differential equation. Another feature that could deserve attention is the possibility of approximating the evolution of a real physical system trajectory to its maximum complexity path. Note that in general, for a real system, the calculation of the maximum complexity path will not be an easy task.

4.2 The Statistical Complexity in the Continuous Case

As explained in the former sections, the LMC statistical measure of complexity [7] identifies the entropy or information stored in a system and its distance to the equilibrium probability distribution, the disequilibrium, as the two ingredients giving the correct asymptotic properties of a well-behaved measure of complexity. In fact, it vanishes both for completely ordered and for completely random systems. Besides giving the main features of an intuitive notion of complexity, it has been shown that LMC complexity successfully enables us to discern situations regarded as complex in discrete systems out of equilibrium: one instance of phase transitions via intermittency in coupled logistic maps [18] or via stochastic synchronization in cellular automata [43], the dynamical behavior of this quantity in a out-equilibrium gases [19, 51, 52] and other applications in classical statistical mechanics [31, 53].

A possible formula of LMC complexity for continuous systems was suggested in formula (4.4). Anteneodo and Plastino [49] pointed out some peculiarities concerning such an extension for continuous probability distributions. It is the aim of this section to offer a discussion of the extension of LMC complexity for continuous systems and to present a slightly modified extension [54] of expression (4.4) that displays interesting and very striking properties. A further generalization of this work has been done in [55, 56].

In Sect. 4.2.1 the extension of information and disequilibrium concepts for the continuous case are discussed. In Sect. 4.2.2 the LMC measure of complexity is reviewed and possible extensions for continuous systems are suggested. We proceed to present some properties of one of these extensions in Sect. 4.2.3.

4.2.1 Entropy/Information and Disequilibrium

Depending on the necessary conditions to fulfill, the extension of an established formula from the discrete to the continuous case always requires a careful study and in many situations some kind of choice between several possibilities. Next we carry out this process for the entropy and disequilibrium formulas.

4.2.1.1 Entropy or Information

As we know, given a discrete probability distribution $\{p_i\}_{i=1,2,\ldots,N}$ satisfying $p_i \geq 0$ and $\sum_{i=1}^{N} p_i = 1$, the *Boltzmann-Gibss-Shannon formula* [4] that accounts for the entropy or information, S, stored in a system is defined by

$$S(\{p_i\}) = -k \sum_{i=1}^{N} p_i \log p_i, \tag{4.38}$$

where k is a positive constant. If we identify H with S, then some properties of this quantity are: (i) *positivity*: $H \geq 0$ for any arbitrary set $\{p_i\}$, (ii) *concavity*: H is concave for arbitrary $\{p_i\}$ and reaches the extremal value for equiprobability ($p_i = 1/N$ $\forall i$), (iii) *additivity*: $H(A \cup B) = H(A) + H(B)$ where A and B are two independent systems, and (iv) *continuity*: H is continuous for each of its arguments. And vice versa, it has been shown that the only function of $\{p_i\}$ verifying the latter properties is given by (4.38) [4, 57]. For an isolated system, the *irreversibility* property is also verified, that is, the time derivative of H is positive, $dH/dt \geq 0$, reaching the equality only for equilibrium.

Calculation of H for a continuous probability distribution $p(x)$, with support on $[-L, L]$ and $\int_{-L}^{L} p(x)\,dx = 1$, can be performed by dividing the interval $[-L, L]$ in small equal-length pieces $\Delta x = x_i - x_{i-1}$, $i = 1, \ldots, n$, with $x_0 = -L$ and $x_n = L$, and by considering the approximated discrete distribution $\{p_i\} = \{p(\bar{x}_i)\Delta x\}$, $i = 1, \ldots, n$, with $\bar{x}_i$ a point in the segment $[x_{i-1}, x_i]$. It gives us

$$\begin{aligned} H^* &= H(\{p_i\}) \\ &= -k \sum_{i=1}^{n} p(\bar{x}_i) \log p(\bar{x}_i) \Delta x - k \sum_{i=1}^{n} p(\bar{x}_i) \log(\Delta x) \Delta x. \end{aligned} \tag{4.39}$$

The second adding term of H^* in the expression (4.39) grows as $\log n$ when n goes to infinity. Therefore it seems reasonable to take just the first and finite adding term of H^* as the extension of H to the continuous case: $H(p(x))$. It characterizes with a finite number the information contained in a continuous distribution $p(x)$. In the limit $n \to \infty$, we obtain

$$\begin{aligned} H(p(x)) &= \lim_{n \to \infty} \left[-k \sum_{i=1}^{n} p(\bar{x}_i) \log p(\bar{x}_i) \Delta x \right] \\ &= -k \int_{-L}^{L} p(x) \log p(x)\,dx. \end{aligned} \tag{4.40}$$

If $p(x) \geq 1$ in some region, the entropy defined by (4.40) can become negative. Although this situation is mathematically possible and coherent, it is unfounded from a physical point of view. See [58] for a discussion on this point. Let $f(p, q)$ be a probability distribution in phase space with coordinates (p, q), $f \geq 0$ and $dp\,dq$ having the dimension of an action. In this case the volume element is $dp\,dq/h$ with h the Planck constant. Suppose that $H(f) < 0$. Because of $\int (dp\,dq/h) f = 1$, the

extent of the region where $f > 1$ must be smaller than h. Hence a negative classical entropy arises if one tries to localize a particle in phase space in a region smaller than h, that is, if the uncertainty relation is violated. In consequence, not every classical probability distribution can be observed in nature. The condition $H(f) = 0$ could give us the minimal width that is physically allowed for the distribution and so the maximal localization of the system under study. This *cutting* property has been used in the calculations performed in [53].

4.2.1.2 Disequilibrium

Given a discrete probability distribution $\{p_i\}_{i=1,2,\ldots,N}$ satisfying $p_i \geq 0$ and $\sum_{i=1}^{N} p_i = 1$, its *Disequilibrium*, D, can be defined as the quadratic distance of the actual probability distribution $\{p_i\}$ to equiprobability:

$$D(\{p_i\}) = \sum_{i=1}^{N} \left(p_i - \frac{1}{N} \right)^2 . \tag{4.41}$$

D is maximal for fully regular systems and vanishes for completely random ones.

In the continuous case with support on the interval $[-L, L]$, the rectangular function $p(x) = 1/(2L)$, with $-L < x < L$, is the natural extension of the equiprobability distribution of the discrete case. The disequilibrium could be defined as

$$D^* = \int_{-L}^{L} \left(p(x) - \frac{1}{2L} \right)^2 dx = \int_{-L}^{L} p^2(x)\, dx - \frac{1}{2L}. \tag{4.42}$$

If we redefine D omitting the constant adding term in D^*, the disequilibrium reads now:

$$D(p(x)) = \int_{-L}^{L} p^2(x)\, dx. \tag{4.43}$$

$D > 0$ for every distribution and it is minimal for the rectangular function which represents the equipartition. D does also tend to infinity when the width of $p(x)$ narrows strongly and becomes extremely peaked.

4.2.2 The Continuous Version $\hat{C}$ of the LMC Complexity

As shown in the previous sections, LMC complexity has been successfully calculated in different systems out of equilibrium. However, Feldman and Crutchfield [21] presented as a main drawback that C vanishes and it is not an extensive variable for finite-memory regular Markov chains when the system size increases. This is not the general behavior of C in the thermodynamic limit as it has been suggested by Calbet and López-Ruiz [19]. On the one hand, when $N \to \infty$ and $k = 1/\log N$, LMC complexity is not a trivial function of the entropy, in the sense that for a given

H there exists a range of complexities between 0 and $C_{\max}(H)$, where $C_{\max}$ is given by expression (4.23).

Observe that in this case H is normalized, $0 < H < 1$, because $k = 1/\log N$. On the other hand, non-extensitivity cannot be considered as an obstacle since it is nowadays well known that there exists a variety of physical systems for which the classical statistical mechanics seems to be inadequate and for which an alternative non-extensive thermodynamics is being hailed as a possible basis of a theoretical framework appropriate to deal with them [59].

According to the discussion in Sect. 4.2.1, the expression of C for the case of a continuum number of states, x, with support on the interval $[-L, L]$ and $\int_{-L}^{L} p(x)\,dx = 1$, is defined by

$$\begin{aligned} C(p(x)) &= H(p(x)) \cdot D(p(x)) \\ &= \left(-k \int_{-L}^{L} p(x) \log p(x)\,dx\right) \cdot \left(\int_{-L}^{L} p^2(x)\,dx\right). \end{aligned} \tag{4.44}$$

Hence, C can become negative. Obviously, $C < 0$ implies $H < 0$. Although this situation is coherent from a mathematical point of view, it is not physically possible. Hence a negative entropy means to localize a system in phase space into a region smaller than h (Planck constant) and this would imply to violate the uncertainty principle (see discussion of Sect. 4.2.1.1). Then a distribution can broaden without any limit but it cannot become extremely peaked. The condition $H = 0$ could indicate the minimal width that $p(x)$ is allowed to have. Similarly to the discrete case, C is positive for any situation and vanishes both for an extreme localization and for the most widely delocalization embodied by the equiprobability distribution. Thus, LMC complexity can be straightforwardly calculated for any continuous distribution by (4.44). Anyway, the positivity of C for every distribution in the continuous case can be recovered by taking the exponential of S [60] and redefining H according to this exponential, i.e. $H = e^S$. To maintain the same nomenclature than in the precedent text we continue to identify H with S and we introduce the symbol $\hat{H} = e^H$. Then the new expression of the statistical measure of complexity C is identified as $\hat{C}$ in the rest of this section and is given by [54]

$$\hat{C}(p(x)) = \hat{H}(p(x)) \cdot D(p(x)) = e^{H(p(x))} \cdot D(p(x)). \tag{4.45}$$

In addition to the positivity, $\hat{C}$ encloses other interesting properties that we describe in the next section.

4.2.3 Properties of $\hat{C}$

The quantity $\hat{C}$ given by (4.45) has been presented as one of the possible extensions of the LMC complexity for continuous systems [54]. We proceed now to present some of the properties that characterize such a complexity indicator.

4.2.3.1 Invariance under Translations and Rescaling Transformations

If $p(x)$ is a density function defined on the real axis $\mathbf{R}$, $\int_{\mathbf{R}} p(x)\,dx = 1$, and $\alpha > 0$ and β are two real numbers, we denote by $p_{\alpha,\beta}(x)$ the new probability distribution obtained by the action of a β-translation and an α-rescaling transformation on $p(x)$,

$$p_{\alpha,\beta}(x) = \alpha p(\alpha(x-\beta)). \tag{4.46}$$

When $\alpha < 1$, $p_{\alpha,\beta}(x)$ broadens whereas if $\alpha > 1$ it becomes more peaked. Observe that $p_{\alpha,\beta}(x)$ is also a density function. After making the change of variable $y = \alpha(x-\beta)$ we obtain

$$\int_{\mathbf{R}} p_{\alpha,\beta}(x)\,dx = \int_{\mathbf{R}} \alpha p(\alpha(x-\beta))\,dx = \int_{\mathbf{R}} p(y)\,dy = 1. \tag{4.47}$$

The behaviour of H under the transformation given by (4.46) is the following:

$$\begin{aligned} H(p_{\alpha,\beta}) &= -\int_{\mathbf{R}} p_{\alpha,\beta}(x)\log p_{\alpha,\beta}(x)\,dx = -\int_{\mathbf{R}} p(y)\log(\alpha p(y))\,dy \\ &= -\int_{\mathbf{R}} p(y)\log p(y)\,dy - \log\alpha \int_{\mathbf{R}} p(y)\,dy \\ &= H(p) - \log\alpha. \end{aligned} \tag{4.48}$$

Then,

$$\hat{H}(p_{\alpha,\beta}) = e^{H(p_{\alpha,\beta})} = \frac{\hat{H}(p)}{\alpha}. \tag{4.49}$$

It is straightforward to see that $D(p_{\alpha,\beta}) = \alpha D(p)$, and to conclude that

$$\hat{C}(p_{\alpha,\beta}) = \hat{H}(p_{\alpha,\beta}) \cdot D(p_{\alpha,\beta}) = \frac{\hat{H}(p)}{\alpha}\alpha D(p) = \hat{C}(p). \tag{4.50}$$

Observe that translations and rescaling transformations keep also the shape of the distributions. Then it could be reasonable to denominate the invariant quantity $\hat{C}$ as the *shape complexity* of the family formed by a distribution $p(x)$ and its transformed $p_{\alpha,\beta}(x)$. Hence, for instance, the rectangular $\Pi(x)$, the isosceles-triangle shaped $\Lambda(x)$, the Gaussian $\Gamma(x)$, or the exponential $\Xi(x)$ distributions continue to belong to the same Π, Λ, Γ or Ξ family, respectively, after applying the transformations defined by (4.46). Calculation of $\hat{C}$ on these distribution families gives us

$$\hat{C}(\Pi) = 1, \tag{4.51}$$

$$\hat{C}(\Lambda) = \frac{2}{3}\sqrt{e} \approx 1.0991, \tag{4.52}$$

$$\hat{C}(\Gamma) = \sqrt{\frac{e}{2}} \approx 1.1658, \tag{4.53}$$

$$\hat{C}(\Xi) = \frac{e}{2} \approx 1.3591. \tag{4.54}$$

Remark that the family of rectangular distributions has a smaller $\hat{C}$ than the rest of distributions. This fact is true for every distribution and it will be proved in Sect. 4.2.3.4.

4.2.3.2 Invariance under Replication

Lloyd and Pagels [15] recommend that a complexity measure should remain essentially unchanged under replication. We show now that $\hat{C}$ is replicant invariant, that is, the shape complexity of m replicas of a given distribution is equal to the shape complexity of the original one.

Suppose $p(x)$ a compactly supported density function, $\int_{-\infty}^{\infty} p(x)\,dx = 1$. Take n copies $p_m(x)$, $m = 1, \ldots, n$, of $p(x)$,

$$p_m(x) = \frac{1}{\sqrt{n}}\, p(\sqrt{n}(x - \lambda_m)), \quad 1 \le m \le n, \tag{4.55}$$

where the supports of all the $p_m(x)$, centered at $\lambda_m' s$ points, $m = 1, \ldots, n$, are all disjoint. Observe that $\int_{-\infty}^{\infty} p_m(x)\,dx = \frac{1}{n}$, what make the union

$$q(x) = \sum_{i=1}^{n} p_m(x) \tag{4.56}$$

to be also a normalized probability distribution, $\int_{-\infty}^{\infty} q(x)\,dx = 1$. For every $p_m(x)$, a straightforward calculation shows that

$$H(p_m) = \frac{1}{n} H(p) + \frac{1}{n} \log \sqrt{n}, \tag{4.57}$$

$$D(p_m) = \frac{1}{n\sqrt{n}} D(p). \tag{4.58}$$

Taking into account that the m replicas are supported on disjoint intervals on $\mathbf{R}$, we obtain

$$H(q) = H(p) + \log \sqrt{n}, \tag{4.59}$$

$$D(q) = \frac{1}{\sqrt{n}} D(p). \tag{4.60}$$

Then,

$$\hat{C}(q) = \hat{C}(p), \tag{4.61}$$

what completes the proof of the replicant invariance of $\hat{C}$.

4.2.3.3 Near-Continuity

Continuity is a desirable property of an indicator of complexity. For a given scale of observation, similar systems should have a similar complexity. In the continuous case, similarity between density functions defined on a common support suggests that they take close values almost everywhere. More strictly speaking, let δ be a positive real number. It will be said that two density functions $f(x)$ and $g(x)$ defined on the interval $I \in \mathbf{R}$ are *δ-neighboring functions* on I if the Lebesgue measure of the points $x \in I$ verifying $|f(x) - g(x)| \ge \delta$ is zero. A real map T defined on density

functions on I will be called *near-continuous* if for any $\varepsilon > 0$ there exists $\delta(\varepsilon) > 0$ such that if $f(x)$ and $g(x)$ are δ-neighboring functions on I then $|T(f) - T(g)| < \varepsilon$.

It can be shown that the information H, the disequilibrium D and the shape complexity $\hat{C}$ are near-continuous maps on the space of density functions defined on a compact support. We must stress at this point the importance of the compactness condition of the support in order to have near-continuity. Take, for instance, the density function defined on the interval $[-1, L]$,

$$g_{\delta,L}(x) = \begin{cases} 1-\delta & \text{if } -1 \le x \le 0, \\ \frac{\delta}{L} & \text{if } 0 \le x \le L, \\ 0 & \text{otherwise,} \end{cases} \tag{4.62}$$

with $0 < \delta < 1$ and $L > 1$. If we calculate H and D for this distribution we obtain

$$H(g_{\delta,L}) = -(1-\delta)\log(1-\delta) - \delta \log\left(\frac{\delta}{L}\right), \tag{4.63}$$

$$D(g_{\delta,L}) = (1-\delta)^2 + \frac{\delta^2}{L}. \tag{4.64}$$

Consider also the rectangular density function

$$\chi_{[-1,0]}(x) = \begin{cases} 1 & \text{if } -1 \le x \le 0, \\ 0 & \text{otherwise.} \end{cases} \tag{4.65}$$

If $0 < \delta < \bar{\delta} < 1$, $g_{\delta,L}(x)$ and $\chi_{[-1,0]}(x)$ are $\bar{\delta}$-neighboring functions. When $\delta \to 0$, we have that $\lim_{\delta\to 0} g_{\delta,L}(x) = \chi_{[-1,0]}(x)$. In this limit process the support is maintained and near-continuity manifests itself as following,

$$\left[\lim_{\delta\to 0} \hat{C}(g_{\delta,L})\right] = \hat{C}(\chi_{[-1,0]}) = 1. \tag{4.66}$$

But if we allow the support L to become infinitely large, the compactness condition is not verified and, although $\lim_{L\to\infty} g_{\delta,L}(x)$ and $\chi_{[-1,0]}(x)$ are $\bar{\delta}$-neighboring distributions, we have that

$$\left[\left(\lim_{L\to\infty} \hat{C}(g_{\delta,L})\right) \to \infty\right] \neq \hat{C}(\chi_{[-1,0]}) = 1. \tag{4.67}$$

Then near-continuity in the map $\hat{C}$ is lost due to the non-compactness of the support when $L \to \infty$. This example suggests that the shape complexity $\hat{C}$ is near-continuous on compact supports and this property will be rigorously proved elsewhere.

4.2.3.4 The Minimal Shape Complexity

If we calculate $\hat{C}$ on the example given by (4.62), we can verify that the shape complexity can be as large as wanted. Take, for instance, $\delta = \frac{1}{2}$. The measure $\hat{C}$ reads now

$$\hat{C}(g_{\delta=\frac{1}{2},L}) = \frac{1}{2}\sqrt{L}\left(1 + \frac{1}{L}\right). \tag{4.68}$$

Thus $\hat{C}$ becomes infinitely large after taking the limits $L \to 0$ or $L \to \infty$. Remark that even in the case $g_{\delta,L}$ has a finite support, $\hat{C}$ is not upper bounded. The density functions, $g_{(\delta=\frac{1}{2}),(L\to 0)}$ and $g_{(\delta=\frac{1}{2}),(L\to\infty)}$, of infinitely increasing complexity have two zones with different probabilities. In the case $L \to 0$ there is a narrow zone where probability rises to infinity and in the case $L \to \infty$ there exists an increasingly large zone where probability tends to zero. Both kind of density functions show a similar pattern to distributions of maximal LMC complexity in the discrete case, where there is an state of dominating probability and the rest of states have the same probability.

The minimal $\hat{C}$ given by (4.68) is found when $L = 1$, that is, when $g_{\delta,L}$ becomes the rectangular density function $\chi_{[-1,1]}$. In fact, the value $\hat{C} = 1$ is the minimum of possible shape complexities and it is reached only on the rectangular distributions. We sketch now some steps that prove this result.

Suppose

$$f = \sum_{k=1}^{n} \lambda_k \chi_{E_k} \tag{4.69}$$

to be a density function consisting of several rectangular pieces E_k, $k = 1, \ldots, n$, on disjoint intervals. If μ_k is the Lebesgue measure of E_k, calculation of $\hat{C}$ gives

$$\hat{C}(f) = \prod_{k=1}^{n} \left(\lambda_k^{-\lambda_k \mu_k}\right) \cdot \left(\sum_{k=1}^{n} \lambda_k^2 \mu_k\right). \tag{4.70}$$

Lagrange multipliers method is used to find the real vector $(\mu_1, \mu_2, \ldots, \mu_n; \lambda_1, \lambda_2, \ldots, \lambda_n)$ that makes extremal the quantity $\hat{C}(f)$ under the condition $\sum_{k=1}^{n} \lambda_k \mu_k = 1$. This is equivalent to studying the extrema of $\log \hat{C}(f)$. We define the function $z(\lambda_k, \mu_k) = \log \hat{C}(f) + \alpha(\sum_{k=1}^{n} \lambda_k \mu_k - 1)$, then

$$z(\lambda_k, \mu_k) = -\sum_{k=1}^{n} \mu_k \lambda_k \log \lambda_k + \log\left(\sum_{k=1}^{n} \mu_k \lambda_k^2\right) + \alpha\left(\sum_{k=1}^{n} \lambda_k \mu_k - 1\right). \tag{4.71}$$

Differentiating this expression and making the result equal to zero we obtain

$$\frac{\partial z(\lambda_k, \mu_k)}{\partial \lambda_k} = -\mu_k \log \lambda_k - \mu_k + \frac{2\lambda_k \mu_k}{\sum_{j=1}^{n} \mu_j \lambda_j^2} + \alpha \mu_k = 0, \tag{4.72}$$

$$\frac{\partial z(\lambda_k, \mu_k)}{\partial \mu_k} = -\lambda_k \log \lambda_k + \frac{\lambda_k^2}{\sum_{j=1}^{n} \mu_j \lambda_j^2} + \alpha \lambda_k = 0. \tag{4.73}$$

Dividing (4.72) by μ_k and (4.73) by λ_k we get

$$\frac{2\lambda_k}{\sum_{j=1}^{n} \mu_j \lambda_j^2} + \alpha - 1 = \log \lambda_k, \tag{4.74}$$

$$\frac{\lambda_k}{\sum_{j=1}^{n} \mu_j \lambda_j^2} + \alpha = \log \lambda_k. \tag{4.75}$$

Solving these two equations for every λ_k we have

$$\lambda_k = \sum_{j=1}^{n} \mu_j \lambda_j^2 \quad \text{for all } k. \tag{4.76}$$

Therefore f is a rectangular function taking the same value λ for every interval E_k, that is, f is the rectangular density function

$$f = \lambda \cdot \chi_L \quad \text{with } \lambda = \frac{1}{\sum_{i=1}^{n} \mu_i} = \frac{1}{L}, \tag{4.77}$$

where L is the Lebesgue measure of the support.

Then $\hat{C}(f) = 1$ is the minimal value for a density function composed of several rectangular pieces because, as we know for the example given by (4.68), $\hat{C}(f)$ is not upper bounded for this kind of distributions.

Furthermore, for every compactly supported density function g and for every $\varepsilon > 0$, it can be shown that near-continuity of $\hat{C}$ allows to find a δ-neighboring density function f of the type given by expression (4.69) verifying $|\hat{C}(f) - \hat{C}(g)| < \varepsilon$. The arbitrariness of the election of ε brings us to conclude that $\hat{C}(g) \geq 1$ for every probability distribution g. Thus, we can conclude that the minimal value of $\hat{C}$ is 1 and it is reached only by the rectangular density functions.

4.3 Fisher-Shannon Information Product. Some Applications

4.3.1 Fisher-Shannon Information: Definition and Properties

The description of electronic properties by means of information measures was introduced into quantum chemistry by the pioneering works [61–65]. In particular Shannon entropy [66] and Fisher information [67] have attracted special attention in atomic and molecular physics. (See e.g. [68–97].) It is known that these two information measures give complementary descriptions of the concentration and uncertainty of the probability density: S_ρ (I_ρ) can be seen as a global (local) measure of spreading. In this context, the Fisher-Shannon information product was found as a link between these information measures to improve the characterization of a probability density function in terms of information measures [77].

The single-electron density, the basic variable of the density functional theory [98] of D-dimensional many-electron systems is given by

$$\rho(\mathbf{r}) = \int |\Psi(\mathbf{r}, \mathbf{r}_2, \ldots, \mathbf{r}_N)|^2 d^D\mathbf{r}_2 \ldots d^D\mathbf{r}_N \tag{4.78}$$

where $\Psi(\mathbf{r}_1, \ldots, \mathbf{r}_N)$ denotes the normalized wavefunction of the N-electron system and $\rho(\mathbf{r})$ is normalized to unity. The spreading of this quantity is best measured by the Shannon information entropy

$$S_\rho = -\int \rho(\mathbf{r}) \ln \rho(\mathbf{r}) d^D\mathbf{r}, \tag{4.79}$$

or equivalently by the Shannon entropy power [60, 66]

$$J_\rho \equiv \frac{1}{2\pi e} e^{\frac{2}{D} S_\rho}. \tag{4.80}$$

On the other hand the Fisher information [60, 67] of $\rho(\mathbf{r})$ is given by

$$I_\rho = \int \frac{|\nabla \rho(\mathbf{r})|^2}{\rho(\mathbf{r})} d^D\mathbf{r}. \tag{4.81}$$

The sharpness, concentration or delocalization of the electronic cloud is measured by both quantities. It is known that these two information measures give complementary descriptions of the smoothness and uncertainty of the electron localization: S_ρ and I_ρ are global and local measures of smoothness, respectively [60–67, 77].

For completeness let us point out that the aforementioned information measures, which refer to an unity-normalized density $\rho_1(\mathbf{r}) \equiv \rho(\mathbf{r})$, are related to the corresponding measures of the N-normalized density $\rho_N(\mathbf{r})$ by

$$S_{\rho_N} = -N \ln N + N S_\rho \quad \text{and} \quad I_{\rho_N} = N I_\rho \tag{4.82}$$

for the Shannon and Fisher quantities, respectively.

The information product concept P_ρ was originally defined in [77] as

$$P_\rho \equiv \frac{1}{D} J_\rho I_\rho, \tag{4.83}$$

and it was applied in the study of electronic properties of quantum systems during last years. (See, e.g. [77, 90, 93, 94, 96, 99–101].) Next we will put forward some mathematical properties which have been obtained in [77, 82, 102, 103] for the Fisher-Shannon information product P_ρ.

4.3.1.1 Scaling Property

The Fisher information and the Shannon entropy power transform as

$$I_{\rho_\gamma} = \gamma^{D-1} I_\rho; \qquad J_{\rho_\gamma} = \gamma^{-(D-1)} J_\rho \tag{4.84}$$

under scaling of the probability density $\rho(\mathbf{r})$ by a real scalar factor γ; i.e. when $\rho_\gamma(\mathbf{r}) = \gamma^D \rho(\gamma \mathbf{r})$. This indicates that they are homogeneous density functionals of degrees 2 and -2, respectively. Consequently, the information product $P_\rho = \frac{1}{D} J_\rho I_\rho$ is invariant under this scaling transformation, i.e.

$$P_{\rho_\gamma} = P_\rho. \tag{4.85}$$

4.3.1.2 Uncertainty Properties

The Fisher information I_ρ and the Shannon entropy power J_ρ satisfy the uncertainty relationship [60]

$$\frac{1}{D} J_\rho I_\rho \geq 1. \tag{4.86}$$

Remark that when one of the involved quantities decreases near to zero, the other has to increase to a large value. Moreover, it is closely linked to the uncertainty relation $\langle r^2\rangle\langle p^2\rangle \geq \frac{D^2}{4}$, where $\langle r^2\rangle$ is defined in terms of the charge position density $\rho(\mathbf{r})$ as $\langle r^2\rangle = \int r^2\rho(\mathbf{r})d^D\mathbf{r}$, and $\langle p^2\rangle$ is given in terms of the momentum density $\Pi(\mathbf{p})$ in an analogous way, where $\Pi(\mathbf{p})$ is defined by means of the Fourier transform of $\Psi(\mathbf{r}_1,\ldots,\mathbf{r}_N)$, $\Phi(\mathbf{p}_1,\ldots,\mathbf{p}_N)$, as

$$\Pi(\mathbf{p}) = \int |\Phi(\mathbf{p},\mathbf{p}_2,\ldots,\mathbf{p}_N)|^2 d^D\mathbf{p}_2\ldots d^D\mathbf{p}_N. \tag{4.87}$$

The Fisher information has been used as a measure of uncertainty in quantum physics. (See e.g. [82, 103–112].) It has been shown to fulfill the Stam inequalities [113]

$$I_\rho \leq 4\langle p^2\rangle; \qquad I_\pi \leq 4\langle r^2\rangle, \tag{4.88}$$

and the Cramer-Rao inequalities [60, 102, 112, 114, 115]

$$I_\rho \geq \frac{D^2}{\langle r^2\rangle}; \qquad I_\pi \geq \frac{D^2}{\langle p^2\rangle} \tag{4.89}$$

for the general single-particle systems. The multiplication of each pair of these inequalities produces

$$\frac{D^4}{\langle r^2\rangle\langle p^2\rangle} \leq I_\rho I_\pi \leq 16\langle r^2\rangle\langle p^2\rangle, \tag{4.90}$$

valid for ground and excited states of general systems, which shows the close connection between the Heisenberg-like uncertainty product and the product of the position and momentum Fisher informations.

Indeed, taken into account $1/D\langle r^2\rangle \geq J_\rho$ [116] one has that

$$\frac{4}{D^2}\langle p^2\rangle\langle r^2\rangle \geq \frac{1}{D}J_\rho I_\rho \geq 1 \tag{4.91}$$

and

$$\frac{4}{D^2}\langle p^2\rangle\langle r^2\rangle \geq \sqrt{P_\rho P_\pi} \geq 1. \tag{4.92}$$

It is straightforward to show that the equality limit of these two inequalities is reached for Gaussian densities.

An special case is given by a single-particle in a central potential. In this framework an uncertainty Fisher information relation was obtained in [103]:

$$I_\rho I_\pi \geq 4D^2\left[1 - \frac{(2l+1)|m|}{2l(l+1)}\right]^2 \tag{4.93}$$

and Fisher information in position space was derived in [82] as

$$I_\rho = 4\langle p^2\rangle - 2(2l+1)|m|\langle r^{-2}\rangle \tag{4.94}$$

where l and m are the orbital and magnetic quantum numbers. Taking into account the duality of the position and momentum spaces as well as the separability of the

wavefunction, one can express the Fisher information of the momentum distribution density as

$$I_\pi = 4\langle r^2\rangle - 2(2l+1)|m|\langle p^{-2}\rangle. \tag{4.95}$$

On the other hand, the radial expectation values $\langle p^2\rangle$ and $\langle r^{-2}\rangle$ ($\langle r^2\rangle$ and $\langle p^{-2}\rangle$) are related [82, 103] by

$$\langle p^2\rangle \geq l(l+1)\langle r^{-2}\rangle, \tag{4.96}$$

$$\langle r^2\rangle \geq l(l+1)\langle p^{-2}\rangle, \tag{4.97}$$

and combining above expressions the fisher uncertainty-like relation (4.93) is obtained.

4.3.1.3 Nonadditivity Properties

The superadditivity of the Fisher information and the subadditivity of the Shannon information of a probability density, can be used to prove [77] that

$$I_W \geq N I_\rho, \tag{4.98}$$

$$S_W \leq N S_\rho, \tag{4.99}$$

where

$$I_W = \int \frac{|\nabla|\Psi(\mathbf{r}_1,\ldots,\mathbf{r}_N)|^2|^2}{|\Psi(\mathbf{r}_1,\ldots,\mathbf{r}_N)|^2} d\mathbf{r}_1\ldots d\mathbf{r}_N \tag{4.100}$$

and

$$S_W = \int |\Psi(\mathbf{r}_1,\ldots,\mathbf{r}_N)|^2 \ln|\Psi(\mathbf{r}_1,\ldots,\mathbf{r}_N)|^2 d\mathbf{r}_1\ldots d\mathbf{r}_N \tag{4.101}$$

for general N-fermion systems in three dimensions. The D-dimensional generalization is obvious. We will show the proof below.

Let $\rho(\mathbf{r})$ a probability density on $\mathbf{R}^t$, that is, $\rho(\mathbf{r})$ non-negative and $\int \rho(\mathbf{r})d\mathbf{r} = 1$. We will suppose that Fisher information and Shannon information of $\rho(\mathbf{r})$ exits. Corresponding to any orthogonal decomposition $\mathbf{R}^t = \mathbf{R}^r \oplus \mathbf{R}^s$, $t = r + s$, the marginal densities are given by:

$$\rho_1(\mathbf{x}) = \int_{\mathbf{R}^r} \rho(\mathbf{x},\mathbf{y})d^r\mathbf{y}, \qquad \rho_2(\mathbf{y}) = \int_{\mathbf{R}^s} \rho(\mathbf{x},\mathbf{y})d^s\mathbf{x} \tag{4.102}$$

then [117]

$$I_\rho \geq I_{\rho_1} + I_{\rho_2} \tag{4.103}$$

property which is known as superadditivity of Fisher information, and

$$S_\rho \leq S_{\rho_1} + S_{\rho_2} \tag{4.104}$$

which is known as subadditivity of Shannon information. Both inequalities saturate when $\rho(\mathbf{x},\mathbf{y}) = \rho_1(\mathbf{x})\rho_2(\mathbf{y})$ [117].

On the other hand, let us consider an N-fermion system and denote the ith-electron density by

$$\rho_i \equiv \rho(\mathbf{r}_i) = \int |\Psi(\mathbf{r}_1, \ldots, \mathbf{r}_i, \ldots, \mathbf{r}_N)|^2 d\mathbf{r}_1 \ldots d\mathbf{r}_{i-1} d\mathbf{r}_{i+1} \ldots d\mathbf{r}_N, \tag{4.105}$$

for $i = 1, \ldots, N$. Then, taken into account that the wavefunction is antisymmetric and (4.103) and (4.104), the wavefunction Fisher information fulfills

$$I_W = \int \frac{|\nabla|\Psi(\mathbf{r}_1, \ldots, \mathbf{r}_N)|^2|^2}{|\Psi(\mathbf{r}_1, \ldots, \mathbf{r}_N)|^2} d\mathbf{r}_1 \ldots d\mathbf{r}_N \geq \sum_{i=1}^{N} I_{\rho_i} = N I_\rho, \tag{4.106}$$

and the wavefunction Shannon information fulfills:

$$S_W = \int |\Psi(\mathbf{r}_1, \ldots, \mathbf{r}_N)|^2 \ln |\Psi(\mathbf{r}_1, \ldots, \mathbf{r}_N)|^2 d\mathbf{r}_1 \ldots d\mathbf{r}_N \leq \sum_{i=1}^{N} S_{\rho_i} = N S_\rho. \tag{4.107}$$

Inequalities (4.106) and (4.107) are equalities when $|\Psi(\mathbf{r}_1, \ldots, \mathbf{r}_N)|^2 = \rho(\mathbf{r_1}) \ldots \rho(\mathbf{r}_N)$.

These properties have allowed us to generalize the following uncertainty relationships:

- The Stam's uncertainty relation for wave functions normalized to unity [77, 113] is generalized via the inequality (4.106) by

$$N I_\rho \leq I_W \leq 4N \langle p^2 \rangle \tag{4.108}$$

- The Shannon information uncertainty relation for wave functions normalized to unity [116] is generalized via inequality (4.107) by

$$\begin{aligned} 3N(1 + \ln \pi) \leq & - \int |\Psi(\mathbf{r}_1, \ldots, \mathbf{r}_N)|^2 \ln |\Psi(\mathbf{r}_1, \ldots, \mathbf{r}_N)|^2 d\mathbf{r}_1 \ldots d\mathbf{r}_N \\ & - \int |\Phi(\mathbf{p}_1, \ldots, \mathbf{p}_N)|^2 \ln |\Phi(\mathbf{p}_1, \ldots, \mathbf{p}_N)|^2 d\mathbf{p}_1 \ldots d\mathbf{p}_N \quad (4.109) \\ \leq & N(S_\rho + S_\pi) \quad (4.110) \end{aligned}$$

  where $S_\rho (S_\pi)$ denotes the Shannon information of the single-particle distribution density in position (momentum) space.

4.3.2 *Fisher-Shannon Product as an Electronic Correlation Measure*

The Fisher-Shannon information product was earlier employed [77] as a tool for studying the electron correlation in atomic systems, in particular in two electron isoelectronic series. The application of this indicator to the electronic shell structure of atoms has received a special attention for systems running from on-electron atoms

to many-electron ones as those corresponding to the periodic table (see, e.g. [93, 94, 96, 99, 102]).

Many electron systems such as atoms, molecules and clusters show the electron correlation phenomenon. This feature has been characterized in terms of the correlation energy [118], which gives the difference between the exact non-relativistic energy and the Hartree-Fock approximation, as well as by some statistical correlation coefficients [119], which asses radial and angular correlation in both the position and momentum density distributions. Some information-theoretic measures of the electron correlation in many electron systems have been proposed during last years [77, 120–130]. Here we will focus on the Fisher-Shannon Information Product as a measure of electron correlation.

The Fisher-Shannon Information Product has been studied in two types of two-electron systems [77] which differ in the Coulomb- and oscillator-like form of the electron-nucleus interaction. The Hamiltonian of such a system is

$$H = -\frac{1}{2}\nabla_1^2 - \frac{1}{2}\nabla_2^2 + V(r_1) + V(r_2) + \frac{1}{|\mathbf{r}_1 - \mathbf{r}_2|}, \tag{4.111}$$

where $V(r_i)$ denotes the electron-nucleus interaction of the ith-electron. $V(r_i) = Z/r_i$ for He-like ions (Z being the nuclear charge) and $V(r_i) = \frac{1}{2}\omega r_i^2$ for the Hooke atoms. The Hooke atom is especially well suited for the understanding of correlation phenomena because of its amenability to analytical treatment.

4.3.2.1 He-Like Ions

In the bare coulomb field case (BCF), i.e. without Coulombic interelectronic interaction in the Hamiltonian, the ground state wave function of He(Z) is a single Slater determinant and the charge density is a hydrogenlike one, so $J_{\rho_Z} = \frac{e}{2\pi^{1/3}}\frac{1}{Z^2}$ and $I_{\rho_Z} = 4Z^2$, so $P_{BCF} = K_{BCF}$ with $K_{BCF} \simeq 1.237333$. To consider the inclusion of electronic interaction we will work with the 204-terms Hylleraas type functions of Koga et al. [131] for the ground states of H^-, He, Li^+, Be^{2+}, B^{3+}, and Ne^{8+} ($Z = 1$–5, 10).

In Fig. 4.16 we have compared the dependence of the information product P_{ρ_Z} on the nuclear charge Z for He-like ions with the bare coulomb field information product. It is apparent the monotonic decrease of P_{ρ_Z} when Z increased, asymptotically approaching the bare or no-correlation value $P_{BCF} = K_{BCF}$ and showing that the electron correlation effect gradually decreases with respect to the electron-nucleus interaction when the nuclear charge of the system is raised up.

4.3.2.2 Hooke's Atoms

For the bare oscillator-field case (BOF), it is known that $J_{\rho_\omega} = 1/(2\omega)$ and $I_{\rho_\omega} = 6\omega$, so that the information product $P_{BOF} = 1$. On the other hand the Schrödinger equation of the entire Hooke atom can be solved analytically for an infinite set of oscillator frequencies [132]. The use of relative and center of mass coordinates allows

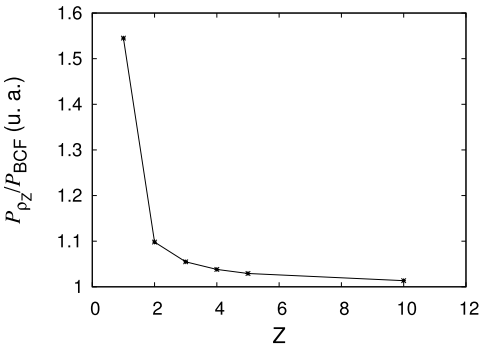

Fig. 4.16 The ratio P_{ρ_Z}/P_{BCF} of the information product for the He-like ions and the information product for bare two-electron atoms as a function of the nuclear charge Z. The points correspond to the values of He(Z) ions with $Z = 1$–5 and 10. The *solid line* has been drawn only to guide the eye

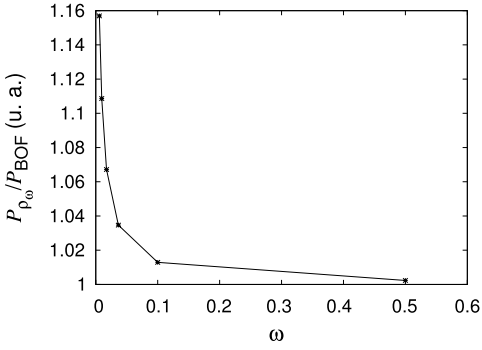

Fig. 4.17 The information product P_{ρ_ω}/P_{BOF} for the Hooke atoms with the oscillator strength $\omega = 0.5$, 0.1, 0.03653727, 0.01734620, 0.009578420, and 0.005841700 and the bare oscillator field information product P_{BOF}. The *solid line* has been drawn only to guide the eye

the Hamiltonian to be separable so that the total wavefunction for singlet states is given by $\Psi(\mathbf{r_1}, \sigma_1, \mathbf{r_2}, \sigma_2) = \xi(\mathbf{R})\Phi(\mathbf{u})\tau(\sigma_1, \sigma_2)$, where $\tau(\sigma_1, \sigma_2)$ is the singlet spin wave function, $\xi(\mathbf{R})$ and $\Phi(\mathbf{u})$ being the solutions of the Schrödinger equations

$$\left(-\frac{1}{4}\nabla_R^2 + \omega R^2\right)\xi(\mathbf{R}) = E_R\xi(\mathbf{R}), \tag{4.112}$$

$$\left(-\nabla_u^2 + \frac{1}{4}\omega u^2 + \frac{1}{u}\right)\Phi(\mathbf{u}) = E_u\Phi(\mathbf{u}), \tag{4.113}$$

respectively, and the total energy $E = E_R + E_u$.

The computed results for the Fisher information and entropy power of these systems are shown in Fig. 4.17 for several ω values, (namely, 0.5, 0.1, 0.03653727, 0.01734620, 0.009578420, and 0.005841700). For these particular values the ground state solution can be obtained [132] as

$$\xi(\mathbf{R}) = \left(\frac{2\omega}{\pi}\right)^{3/4} e^{-\omega R^2} \quad \text{and} \quad \Phi(\mathbf{u}) = e^{-\frac{\omega r^2}{4}} Q_n(r) \tag{4.114}$$

where $Q_n(r)$ is a polynomial whose coefficients can be determined analytically.

Cioslowski et al. [133] quantify the domains of the weakly correlated regime of this system which corresponds to the values of ω greater than $\omega_c \simeq 4.011624 \times 10^{-2}$, and the strongly correlated regime that encompasses the values of ω smaller than ω_c.

In Fig. 4.17 we have drawn P_{ρ_ω}/P_{BOF} as a function of the oscillator electron-nucleus strength ω. It is apparent that the value of the electron density functional P_{ρ_ω}/P_{BOF} (dots) is always bigger than unity, when the electron-electron repulsion becomes very small with respect to the oscillator electron-nucleus interaction, the points approach to the value 1, indicating the decrease of the relative importance of electron correlation when the strength ω is increased.

4.3.3 Fisher Information for a Single Particle in a Central Potential

As another application, let us consider the Fisher information in the position space (for momentum space is analogous) of a single-particle system in a central potential $V(r)$, defined by

$$I_\rho = \int \frac{|\nabla\rho(\mathbf{r})|^2}{\rho(\mathbf{r})} d\mathbf{r} \tag{4.115}$$

where $\rho(\mathbf{r}) = |\psi(\mathbf{r})|^2$ and where $\psi(\mathbf{r})$ is the bound solutions of the Schrödinger equation

$$\left[-\frac{1}{2}\nabla^2 + V(r)\right]\psi(\mathbf{r}) = E\psi(\mathbf{r}). \tag{4.116}$$

For bounded states the solution of above equation is given by

$$\psi_{nlm}(\mathbf{r}) = R_{nl}(r)Y_{lm}(\Omega) \tag{4.117}$$

where $R_{nl}(r)$ is the radial part of the function and $Y_{lm}(\Omega)$ is the spherical harmonic of order l that is given by

$$Y_{lm}(\Omega) = \frac{1}{\sqrt{2\pi}} e^{im\phi}\Theta_{lm}(\cos\theta) \quad (-l \le m \le l \text{ and } 0 \le \theta \le \pi,\ 0 \le \phi \le 2\pi) \tag{4.118}$$

where $\Theta_{lm}(x)$ are given in terms of the associated Legendre functions of the first kind $P_l^m(x)$:

$$\Theta_{lm}(x) = \sqrt{\frac{2l+1}{2}\frac{(l-m)!}{(l+m)!}} P_l^m(x). \tag{4.119}$$

So the Fisher information for a single particle in a central potential is given by

$$\begin{aligned} I_{\rho_{nlm}} &= 4\int |\nabla\rho_{nlm}^{1/2}(\mathbf{r})|^2 \\ &= \int \left[\Theta_{lm}^2(\theta)\left(\frac{\partial R_{nl}^2(r)}{\partial r}\right)^2 + \frac{1}{r^2}R_{nl}^2(r)\left(\frac{\partial\Theta_{lm}(\theta)}{\partial\theta}\right)^2\right] d\mathbf{r}, \end{aligned} \tag{4.120}$$

on the other hand the kinetic energy is given by:

$$\langle p^2\rangle_{nlm} = \int |\nabla\psi_{nlm}(\mathbf{r})|^2 = \int \left[\left(\frac{\partial R_{nl}(r)}{\partial r}\right)^2 |Y_{lm}(\Omega)|^2\right] d\mathbf{r} + \int \left[\frac{1}{r^2} R_{nl}^2(r)\left(\frac{\partial \Theta_{lm}(\theta)}{\partial\theta}\right)^2 + \frac{1}{r^2}\frac{1}{\sin^2\theta} R_{nl}^2(r)\Theta_{lm}^2(\theta)m^2\right] d\mathbf{r} \tag{4.121}$$

thus

$$I_{\rho_{nlm}} = 4\langle p^2\rangle_{nlm} - 2\langle r^{-2}\rangle_{nlm}(2l+1)|m|. \tag{4.122}$$

4.3.3.1 Hydrogen Atom

For this system the potential is $V(r) = -1/r$ and the expectation values $\langle p^2\rangle_{nlm} = \frac{1}{n^2}$ and $\langle r^{-2}\rangle_{nlm} = \frac{2}{(2l+1)n^3}$ thus

$$I_{\rho_{nlm}} = \frac{4}{n^2}\left(1 - \frac{|m|}{n}\right). \tag{4.123}$$

4.3.3.2 Isotropic Harmonic Oscillator

In this case the potential is $V(r) = \frac{1}{2}\omega^2 r^2$ and the expectation values $\langle p^2\rangle_{nlm} = \omega(2n + l + \frac{3}{2})$ and $\langle r^{-2}\rangle_{nlm} = \frac{\omega}{(2l+1)}$

$$I_{\rho_{nlm}} = 4\omega\left(2n + l + \frac{3}{2} - |m|\right). \tag{4.124}$$

4.4 Applications to Quantum Systems

4.4.1 Formulas in Position and Momentum Spaces

Here, we summarize the formulas and the nomenclature that will use in all this section.

The measure of complexity C has been defined as

$$C = H \cdot D, \tag{4.125}$$

where H represents the information content of the system and D gives an idea of how much concentrated is its spatial distribution.

The simple exponential Shannon entropy, in the position and momentum spaces, takes the form, respectively,

$$H_r = e^{S_r}, \qquad H_p = e^{S_p}, \tag{4.126}$$

where S_r and S_p are the Shannon information entropies,

$$S_r = -\int \rho(\mathbf{r}) \log \rho(\mathbf{r})\, d\mathbf{r}, \qquad S_p = -\int \gamma(\mathbf{p}) \log \gamma(\mathbf{p})\, d\mathbf{p}, \tag{4.127}$$

and $\rho(\mathbf{r})$ and $\gamma(\mathbf{p})$ are the densities normalized to 1 of the quantum system in position and momentum spaces, respectively.

The disequilibrium is:

$$D_r = \int \rho^2(\mathbf{r})\, d\mathbf{r}, \qquad D_p = \int \gamma^2(\mathbf{p})\, d\mathbf{p}. \tag{4.128}$$

In this manner, the final expressions for C in position and momentum spaces are:

$$C_r = H_r \cdot D_r, \qquad C_p = H_p \cdot D_p. \tag{4.129}$$

Second, the Fisher-Shannon information, P, in the position and momentum spaces, is given respectively by

$$P_r = J_r \cdot I_r, \qquad P_p = J_p \cdot I_p, \tag{4.130}$$

where the first factor

$$J_r = \frac{1}{2\pi e} e^{2S_r/3}, \qquad J_p = \frac{1}{2\pi e} e^{2S_p/3}, \tag{4.131}$$

is a version of the exponential Shannon entropy, and the second factor

$$I_r = \int \frac{[\nabla \rho(\mathbf{r})]^2}{\rho(\mathbf{r})}\, d\mathbf{r}, \qquad I_p = \int \frac{[\nabla \gamma(\mathbf{p})]^2}{\gamma(\mathbf{p})}\, d\mathbf{p}, \tag{4.132}$$

is the Fisher information measure, that quantifies the narrowness of the probability density.

4.4.2 The H-atom

The atom can be considered a complex system. Its structure is determined through the well established equations of Quantum Mechanics [134, 135]. Depending on the set of quantum numbers defining the state of the atom, different conformations are available to it. As a consequence, if the wave function of the atomic state is known, the probability densities in the position and the momentum spaces are obtained, and from them, the different statistical magnitudes such as Shannon and Fisher informations, different indicators of complexity, etc., can be calculated.

These quantities enlighten new details of the hierarchical organization of the atomic states. In fact, states with the same energy can display, for instance, different values of complexity. This is the behavior shown by the simplest atomic system, that is, the hydrogen atom (H-atom). Now, we present the calculations for this system [94].

The non-relativistic wave functions of the H-atom in position space ($\mathbf{r} = (r, \Omega)$, with r the radial distance and Ω the solid angle) are:

$$\Psi_{n,l,m}(\mathbf{r}) = R_{n,l}(r) Y_{l,m}(\Omega), \tag{4.133}$$

where $R_{n,l}(r)$ is the radial part and $Y_{l,m}(\Omega)$ is the spherical harmonic of the atomic state determined by the quantum numbers (n, l, m). The radial part is expressed as [135]

$$R_{n,l}(r) = \frac{2}{n^2}\left[\frac{(n-l-1)!}{(n+l)!}\right]^{1/2}\left(\frac{2r}{n}\right)^l e^{-\frac{r}{n}} L_{n-l-1}^{2l+1}\left(\frac{2r}{n}\right), \tag{4.134}$$

being $L_\alpha^\beta(t)$ the associated Laguerre polynomials. Atomic units are used here.

The same functions in momentum space ($\mathbf{p} = (p, \hat{\Omega})$, with p the momentum modulus and $\hat{\Omega}$ the solid angle) are:

$$\hat{\Psi}_{n,l,m}(\mathbf{p}) = \hat{R}_{n,l}(p) Y_{l,m}(\hat{\Omega}), \tag{4.135}$$

where the radial part $\hat{R}_{n,l}(p)$ is now given by the expression [136]

$$\hat{R}_{n,l}(p) = \left[\frac{2}{\pi}\frac{(n-l-1)!}{(n+l)!}\right]^{1/2} n^2 2^{2l+2} l! \frac{n^l p^l}{(n^2p^2+1)^{l+2}} C_{n-l-1}^{l+1}\left(\frac{n^2p^2-1}{n^2p^2+1}\right), \tag{4.136}$$

with $C_\alpha^\beta(t)$ the Gegenbauer polynomials.

Taking the former expressions, the probability density in position and momentum spaces,

$$\rho(\mathbf{r}) = |\Psi_{n,l,m}(\mathbf{r})|^2, \qquad \gamma(\mathbf{p}) = |\hat{\Psi}_{n,l,m}(\mathbf{p})|^2, \tag{4.137}$$

can be explicitly calculated. From these densities, the statistical complexity and the Fisher-Shannon information are computed.

C_r and C_p (see expression (4.129)) are plotted in Fig. 4.18 as function of the modulus of the third component m of the orbital angular momentum l for different pairs of (n, l) values. The range of the quantum numbers is: $n \geq 1$, $0 \leq l \leq n-1$, and $-l \leq m \leq l$. Figure 4.18(a) shows C_r for $n = 15$ and Fig. 4.18(b) shows C_r for $n = 30$. In both figures, it can be observed that C_r splits in different sets of discrete points. Each one of these sets is associated to a different l value. It is worth to note that the set with the minimum values of C_r corresponds just to the highest l, that is, $l = n-1$. The same behavior can be observed in Figs. 4.18(c) and 4.18(d) for C_p.

Figure 4.19 shows the calculation of P_r and P_p (see expression (4.130)) as function of the modulus of the third component m for different pairs of (n, l) values. The second factor, I_r or I_p, of this indicator can be analytically obtained in both spaces (position and momentum). The results are [82]:

$$I_r = \frac{4}{n^2}\left(1 - \frac{|m|}{n}\right), \tag{4.138}$$

$$I_p = 2n^2\left\{5n^2 + 1 - 3l(l+1) - (8n - 3(2l+1))|m|\right\}. \tag{4.139}$$

In Fig. 4.19(a), P_r is plotted for $n = 15$, and P_r is plotted for $n = 30$ in Fig. 4.19(b). Here P_r also splits in different sets of discrete points, showing a behavior parallel to the above signaled for C (Fig. 4.18). Each one of these sets is also related with a different l value. It must be remarked again that the set with the minimum values of P_r corresponds just to the highest l. In Figs. 4.19(c) and 4.19(d), the same behavior can be observed for P_p.

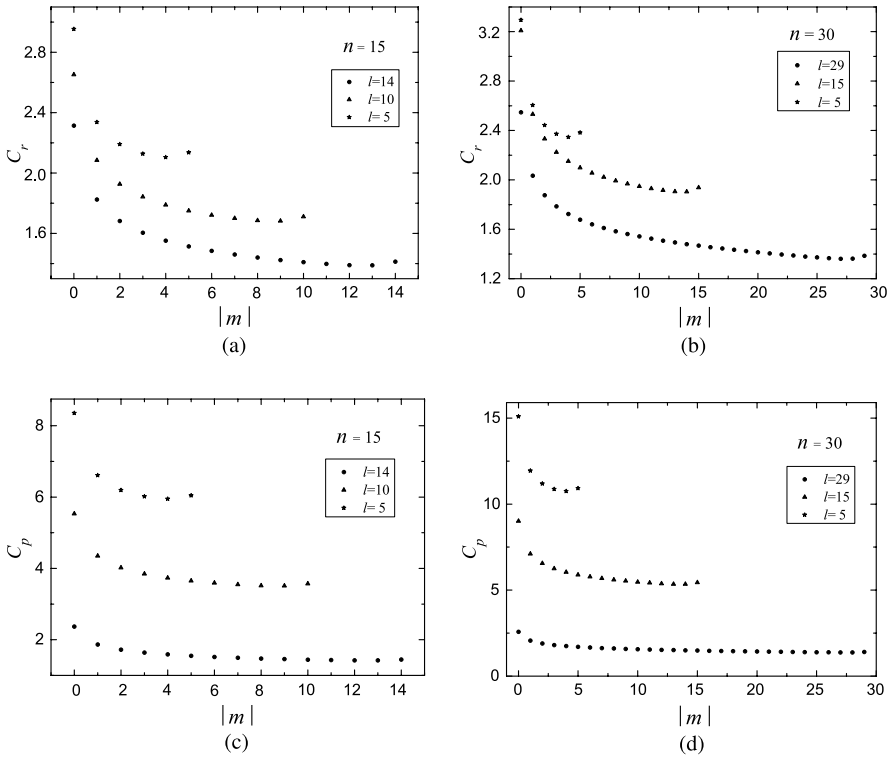

Fig. 4.18 Statistical complexity in position space, C_r, and momentum space, C_p, vs. $|m|$ for different (n, l) values in the hydrogen atom. C_r for (**a**) $n = 15$ and (**b**) $n = 30$. C_p for (**c**) $n = 15$ and (**d**) $n = 30$. All values are in atomic units

Then, it is put in evidence that, for a fixed level of energy n, these statistical magnitudes take their minimum values for the highest allowed orbital angular momentum, $l = n - 1$. It is worth to remember at this point that the mean radius of an $(n, l = n - 1)$ orbital, $\langle r \rangle_{n,l}$, is given by [137]

$$\langle r \rangle_{n,l=n-1} = n^2 \left(1 + \frac{1}{2n} \right), \tag{4.140}$$

that tends, when n is very large, to the radius of the nth energy level, $r_{Bohr} = n^2$, of the Bohr atom. The radial part of this particular wave function, that describes the electron in the $(n, l = n - 1)$ orbital, has no nodes. In fact, if we take the standard deviation, $(\Delta r) = \langle (r - \langle r \rangle)^2 \rangle^{1/2}$, of this wave function, $(\Delta r) = n\sqrt{2n+1}/2$, the ratio $(\Delta r)/\langle r \rangle$ becomes $1/\sqrt{2n}$ for large n. This means that the spatial configuration of this atomic state is like a spherical shell that converges to a semiclassical Bohr-like orbit when n tends to infinity. These highly excited H-atoms are referred as Rydberg atoms, that have been intensively studied [138] for its importance in areas as astrophysics, plasma physics, quantum optics, etc., and also in studies of the classical limit of quantum mechanics [139].

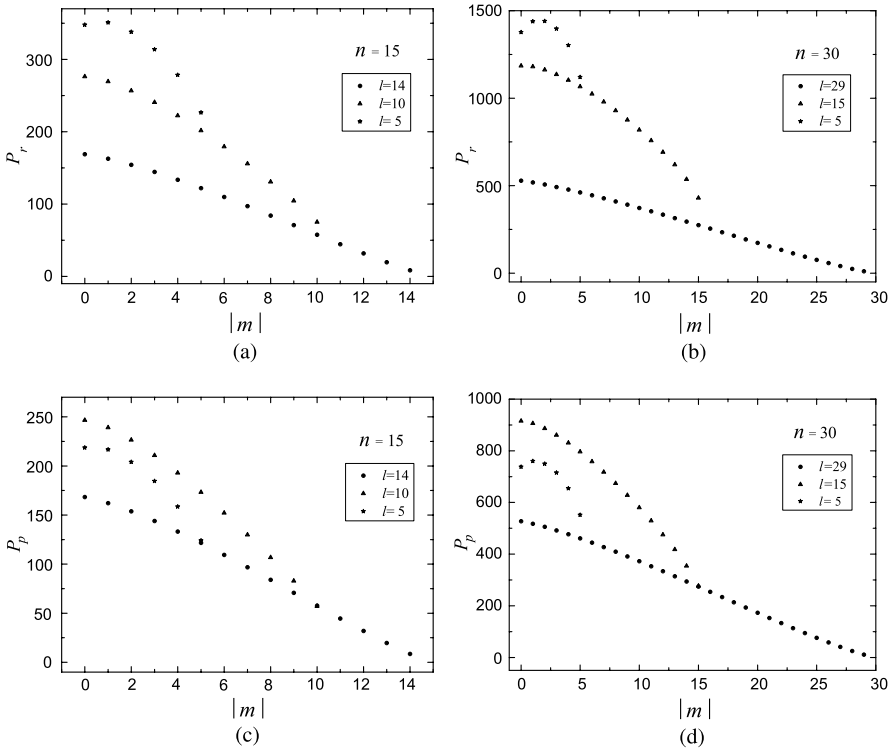

Fig. 4.19 Fisher-Shannon information in position space, P_r, and momentum space, P_p, vs. $|m|$ for different (n, l) values in the hydrogen atom. P_r for (**a**) $n = 15$ and (**b**) $n = 30$. P_p for (**c**) $n = 15$ and (**d**) $n = 30$. All values are in atomic units

We conclude this section by remarking that the minimum values of these statistical measures calculated from the quantum wave functions of the H-atom enhance our intuition by selecting just those orbitals that for a large principal quantum number converge to the Bohr-like orbits in the pre-quantum image. Therefore, these results show that insights on the structural conformation of quantum systems can be inferred from these magnitudes, as it can also be seen in the next sections.

4.4.3 The Quantum Harmonic Oscillator

As suggested in the previous section, a variational process on the statistical measures calculated in the H-atom could select just those orbitals that in the pre-quantum image are the Bohr-like orbits. Now, we show that a similar behavior for the statistical complexity and Fisher-Shannon information is also found in the case of the isotropic quantum harmonic oscillator [93].

We recall the three-dimensional non-relativistic wave functions of this system when the potential energy is written as $V(r) = \lambda^2 r^2/2$, with λ a positive real con-

stant expressing the potential strength. In the same way as in the H-atom (4.133), these wave functions in position space ($\mathbf{r} = (r, \Omega)$, with r the radial distance and Ω the solid angle) are:

$$\Psi_{n,l,m}(\mathbf{r}) = R_{n,l}(r) Y_{l,m}(\Omega), \tag{4.141}$$

where $R_{n,l}(r)$ is the radial part and $Y_{l,m}(\Omega)$ is the spherical harmonic of the quantum state determined by the quantum numbers (n, l, m). Atomic units are used here. The radial part is expressed as [140]

$$R_{n,l}(r) = \left[\frac{2n!\lambda^{l+3/2}}{\Gamma(n+l+3/2)}\right]^{1/2} r^l e^{-\frac{\lambda}{2}r^2} L_n^{l+1/2}(\lambda r^2), \tag{4.142}$$

where $L_\alpha^\beta(t)$ are the associated Laguerre polynomials. The levels of energy are given by

$$E_{n,l} = \lambda(2n + l + 3/2) = \lambda(e_{n,l} + 3/2), \tag{4.143}$$

where $n = 0, 1, 2, \ldots$ and $l = 0, 1, 2, \ldots$. Let us observe that $e_{n,l} = 2n + l$. Thus, different pairs of (n, l) can give the same $e_{n,l}$, and then the same energy $E_{n,l}$.

The wave functions in momentum space ($\mathbf{p} = (p, \hat{\Omega})$, with p the momentum modulus and $\hat{\Omega}$ the solid angle) present the same form as in the H-atom (4.135):

$$\hat{\Psi}_{n,l,m}(\mathbf{p}) = \hat{R}_{n,l}(p) Y_{l,m}(\hat{\Omega}), \tag{4.144}$$

where the radial part $\hat{R}_{n,l}(p)$ is now given by the expression [140]

$$\hat{R}_{n,l}(p) = \left[\frac{2n!\lambda^{-l-3/2}}{\Gamma(n+l+3/2)}\right]^{1/2} p^l e^{-\frac{p^2}{2\lambda}} L_n^{l+1/2}(p^2/\lambda). \tag{4.145}$$

Taking the former expressions, the probability density in position and momentum spaces,

$$\rho_\lambda(\mathbf{r}) = |\Psi_{n,l,m}(\mathbf{r})|^2, \qquad \gamma_\lambda(\mathbf{p}) = |\hat{\Psi}_{n,l,m}(\mathbf{p})|^2, \tag{4.146}$$

can be explicitly calculated. From these densities, the statistical complexity (see expression (4.129)) and the Fisher-Shannon information (see expression (4.130)) are computed. It is shown in Sect. 4.4.3.1 that these quantities are independent of λ, the potential strength, and also that they are the same in both position and momentum spaces, i.e. $C_r = C_p$ and $P_r = P_p$.

In Fig. 4.20, C_r (or C_p) is plotted as function of the modulus of the third component m, $-l \leq m \leq l$, of the orbital angular momentum l for different l values with a fixed energy. That is, according to expression (4.143), the quantity $e_{n,l} = 2n + l$ is constant in each figure. Figure 4.20(a) shows C_r for $e_{n,l} = 15$ and Fig. 4.20(b) shows C_r for $e_{n,l} = 30$. In both figures, it can be observed that C_r splits in different sets of discrete points. Each one of these sets is associated to a different l value. It is worth noting that the set with the minimum values of C_r corresponds just to the highest l, that is, $l = 15$ in Fig. 4.20(a) and $l = 30$ in Fig. 4.20(b).

Figure 4.21 shows P as function of the modulus of the third component m for different pairs of $(e_{n,l} = 2n + l, l)$ values. The second factor, I_r or I_p, of this indicator can be analytically obtained in both spaces (position and momentum) [82]:

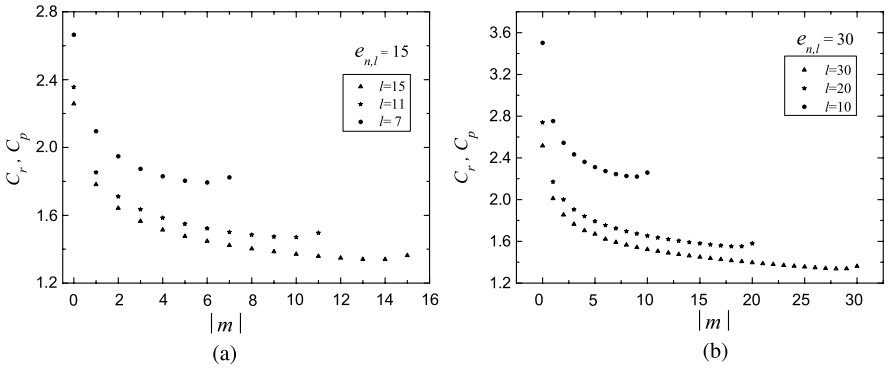

Fig. 4.20 Statistical complexity in position space, C_r, and momentum space, C_p, vs. $|m|$ for different energy $e_{n,l}$-values in the quantum isotropic harmonic oscillator for (**a**) $e_{n,l} = 15$ and (**b**) $e_{n,l} = 30$. Recall that $C_r = C_p$. All values are in atomic units

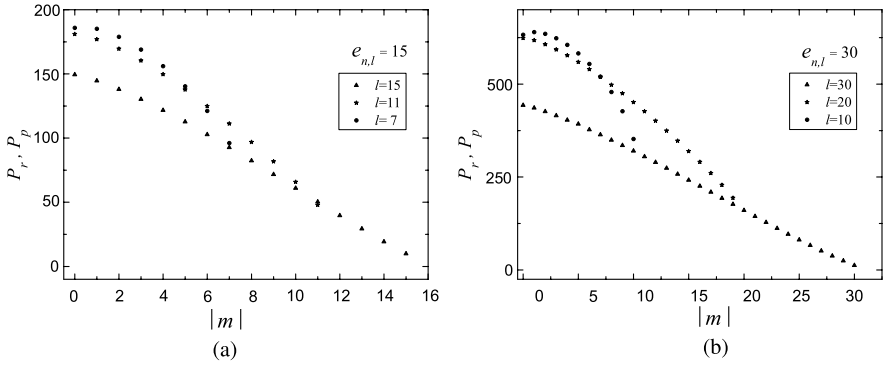

Fig. 4.21 Fisher-Shannon information in position space, P_r, and momentum space, P_p, vs. $|m|$ for different energy $e_{n,l}$-values in the quantum isotropic harmonic oscillator for (**a**) $e_{n,l} = 15$ and (**b**) $e_{n,l} = 30$. Recall that $P_r = P_p$. All values are in atomic units

$$I_r = 4(2n + l + 3/2 - |m|)\lambda, \tag{4.147}$$

$$I_p = 4(2n + l + 3/2 - |m|)\lambda^{-1}. \tag{4.148}$$

Let us note that I_r and I_p depend on λ, although the final result for P_r and P_p are non λ-dependent (see Sect. 4.4.3.1). In Fig. 4.21(a), P_r (or P_p) is plotted for $e_{n,l} = 15$, and P_r is plotted for $e_{n,l} = 30$ in Fig. 4.21(b). Here, P_r also splits in different sets of discrete points, showing a behavior similar to that of C in Fig. 4.20. Each one of these sets is related with a different l value, and the set with the minimum values of P_r also corresponds just to the highest l, that is, $l = 15$ and $l = 30$, respectively.

As in the H-atom, we also see here that, for a fixed level of energy, let us say $e_{n,l} = 2n + l$, these statistical quantities take their minimum values for the highest allowed orbital angular momentum, $l = e_{n,l}$. It is worth remembering at this point that the radial part of this particular wave function, that describes the quan-

tum system in the $(n=0, l=e_{n,l})$ orbital, has no nodes. This means that the spatial configuration of this state is, in some way, a spherical-like shell. In Sect. 4.4.3.2, the mean radius of this shell, $\langle r\rangle_{n,l,m}$, is found for the case $(n=0, l=e_{n,l}, m)$. This is:

$$\langle r\rangle_{n=0,l=e_{n,l},m} \equiv \langle r\rangle_{n=0,l=e_{n,l}} \simeq \sqrt{\lambda^{-1}(e_{n,l}+1)}\left(1+\Theta(e_{n,l}^{-1})\right), \tag{4.149}$$

that tends, when $e_{n,l} \gg 1$, to the radius of the Nth energy level, $r_N = \sqrt{\lambda^{-1}(N+1)}$, taking $N = e_{n,l}$ in the Bohr-like picture of the harmonic oscillator (see Sect. 4.4.3.2).

Then, we can remark again that the minimum values of the statistical measures calculated from the wave functions of the quantum isotropic harmonic oscillator also select just those orbitals that in the pre-quantum image are the Bohr-like orbits.

4.4.3.1 Invariance of C and P under Rescaling Transformations

Here, it is shown that the statistical complexities C_r and C_p are equal and independent of the strength potential, λ, for the case of the quantum isotropic harmonic oscillator. Also, the same behavior is displayed by P_r and P_p.

For a fixed set of quantum numbers, (n, l, m), let us define the normalized probability density $\hat{\rho}(\mathbf{t})$:

$$\hat{\rho}(\mathbf{t}) = \frac{2n!}{\Gamma(n+l+3/2)} t^{2l} e^{-t^2} \left[L_n^{l+1/2}(t^2)\right]^2 |Y_{l,m}(\Omega)|^2. \tag{4.150}$$

From expressions (4.141), (4.142) and (4.146), it can be obtained that

$$\rho_\lambda(\mathbf{r}) = \lambda^{3/2}\hat{\rho}(\lambda^{1/2}\mathbf{r}), \tag{4.151}$$

where ρ_λ is the normalized probability density of expression (4.146). Now, it is straightforward to find that

$$H_r(\rho_\lambda) = \lambda^{-3/2} H(\hat{\rho}), \tag{4.152}$$

and that

$$D_r(\rho_\lambda) = \lambda^{3/2} D(\hat{\rho}). \tag{4.153}$$

Then,

$$C_r(\rho_\lambda) = C(\hat{\rho}), \tag{4.154}$$

and the non λ-dependence of C_r is shown.

To show that C_r and C_p are equal, let us note that, from expressions (4.144), (4.145) and (4.146), the normalized probability density $\gamma_\lambda(\mathbf{p})$ for the same set of quantum numbers (n, l, m) can be written as

$$\gamma_\lambda(\mathbf{p}) = \lambda^{-3/2}\hat{\rho}(\lambda^{-1/2}\mathbf{p}). \tag{4.155}$$

Now, it is found that

$$H_p(\gamma_\lambda) = \lambda^{3/2} H(\hat{\rho}), \tag{4.156}$$

and that

$$D_p(\gamma_\lambda) = \lambda^{-3/2} D(\hat{\rho}). \tag{4.157}$$

Then,

$$C_p(\gamma_\lambda) = C(\hat{\rho}), \tag{4.158}$$

and the equality of C_r and C_p, and their non λ-dependence are shown.

Similarly, from expressions (4.130), (4.131), (4.147) and (4.148), it can be found that $P_r = P_p$, and that these quantities are also non λ-dependent.

4.4.3.2 Bohr-Like Orbits in the Quantum Isotropic Harmonic Oscillator

Here, the mean radius of the orbital with the lowest complexity is calculated as function of the energy. Also, the radii of the orbits in the Bohr picture are obtained.

The general expression of the mean radius of a state represented by the wave function $\Psi_{n,l,m}$ is given by

$$\langle r \rangle_{n,l,m} \equiv \langle r \rangle_{n,l} = \frac{n!}{\Gamma(n+l+3/2)} \frac{1}{\lambda^{1/2}} \int_0^\infty t^{l+1} e^{-t} \left[L_n^{l+1/2}(t) \right]^2 dt. \tag{4.159}$$

For the case of minimum complexity (see Figs. 4.20 or 4.21), the state has the quantum numbers $(n = 0, l = e_{n,l})$. The last expression (4.159) becomes:

$$\langle r \rangle_{n=0,l=e_{n,l}} = \frac{(e_{n,l}+1)!}{\Gamma(e_{n,l}+3/2)\lambda^{1/2}}, \tag{4.160}$$

that, in the limit $e_{n,l} \gg 1$, simplifies to expression (4.149):

$$\langle r \rangle_{n=0,l=e_{n,l}\gg 1} \simeq \sqrt{\lambda^{-1}(e_{n,l}+1)} \left(1 + \Theta(e_{n,l}^{-1})\right). \tag{4.161}$$

Now we obtain the radius of an orbit in the Bohr-like image of the isotropic harmonic oscillator. Let us recall that this image establishes the quantization of the energy through the quantization of the classical orbital angular momentum. So, the energy E of a particle of mass m moving with velocity v on a circular orbit of radius r under the harmonic potential $V(r) = m\lambda^2 r^2/2$ is:

$$E = \frac{1}{2} m\lambda^2 r^2 + \frac{1}{2} m v^2. \tag{4.162}$$

The circular orbit is maintained by the central force through the equation:

$$\frac{mv^2}{r} = m\lambda^2 r. \tag{4.163}$$

The angular momentum takes discrete values according to the condition

$$mvr = (N+1)\hbar \quad (N = 0, 1, 2, \ldots). \tag{4.164}$$

Combining the last three equations (4.162)–(4.164), and taking atomic units, $m = \hbar = 1$, the radius r_N of a Bohr-like orbit for this system is obtained

$$r_N = \sqrt{\lambda^{-1}(N+1)} \quad (N = 0, 1, 2, \ldots). \tag{4.165}$$

Let us observe that this expression coincides with the quantum mechanical radius given by expression (4.161) when $e_{n,l} = N$ for $N \gg 1$.

4.4.4 The Square Well

Statistical complexity has been calculated in different atomic systems, such as in the H atom (Sect. 4.4.2) and in the quantum harmonic oscillator (Sect. 4.4.3). The behavior of this statistical magnitude in comparison with that of the energy displays some differences. Among other applications, the energy has a clear physical meaning [134] and it can be used to find the equilibrium states of a system. In the same way, it has also been shown that the complexity can give some insight about the equilibrium configuration in the ground state of the H_2^+ molecule [100]. In this case, Montgomery and Sen have reported that the minimum of the statistical complexity as a function of the internuclear distance for this molecule is an accurate result comparable with that obtained with the minimization of the energy. This fact could suggest that energy and complexity are two magnitudes strongly correlated for any quantum system. But this is not the general case. See, for example, the behavior of both magnitudes in the previous sections for the H-atom and for the quantum isotropic harmonic oscillator. In both systems, the degeneration of the energy is split by the statistical complexity, in such a way that the minimum of complexity for each level of energy is taken on the wave function with the maximum orbital angular momentum. Therefore, energy and complexity are two independent variables.

In this section, we wonder if there exists a quantum system where degeneration of the complexity can be split by the energy. The answer will be affirmative [141]. We show it in two steps. First, a new type of invariance by replication for the statistical complexity is established, and, second, it is seen that the energy eigenstates of the quantum infinite square well fulfill the requirements of this kind of invariance. From there, it is revealed that the degeneration of complexity in this quantum system is broken by the energy.

Different types of replication can be defined on a given probability density. One of them was established in [54]. Here, a similar kind of replication is presented, in such a manner that the complexity C of m replicas of a given distribution is equal to the complexity of the original one. Thus, if $\mathbf{R}$ represents the support of the density function $p(x)$, with $\int_{\mathbf{R}} p(x)\,dx = 1$, take n copies $p_m(x)$, $m = 1, \ldots, n$, of $p(x)$,

$$p_m(x) = p(n(x - \lambda_m)), \quad 1 \leq m \leq n, \tag{4.166}$$

where the supports of all the $p_m(x)$, centered at $\lambda_m' s$ points, $m = 1, \ldots, n$, are all disjoint. Observe that $\int_{\mathbf{R}} p_m(x)\,dx = \frac{1}{n}$, what makes the replicas union

$$q_n(x) = \sum_{i=1}^{n} p_m(x) \tag{4.167}$$

to be also a normalized probability distribution, $\int_{\mathbf{R}} q_n(x)\,dx = 1$. For every $p_m(x)$, a straightforward calculation shows that the Shannon entropy is

$$S(p_m) = \frac{1}{n} S(p), \tag{4.168}$$

and the disequilibrium is

$$D(p_m) = \frac{1}{n} D(p). \tag{4.169}$$

Taking into account that the m replicas are supported on disjoint intervals on $\mathbf{R}$, we obtain

$$S(q_n) = S(p), \tag{4.170}$$

$$D(q_n) = D(p). \tag{4.171}$$

Then, the statistical complexity ($C = e^S \cdot D$) is

$$C(q_n) = C(p), \tag{4.172}$$

and this type of invariance by replication for C is shown.

Let us see now that the probability density of the eigenstates of the energy in the quantum infinite square well display this type of invariance. The wave functions representing these states for a particle in a box, that is confined in the one-dimensional interval $[0, L]$, are given by [142]

$$\varphi_k(x) = \sqrt{\frac{2}{L}} \sin\left(\frac{k\pi x}{L}\right), \quad k = 1, 2, \ldots. \tag{4.173}$$

Taking $p(x)$ as the probability density of the fundamental state ($k = 1$),

$$p(x) = |\varphi_1(x)|^2, \tag{4.174}$$

the probability density of the kth excited state,

$$q_k(x) = |\varphi_k(x)|^2, \tag{4.175}$$

can be interpreted as the union of k replicas of the fundamental state density, $p(x)$, in the k disjoint intervals $[(m-1)L/k, mL/k]$, with $m = 1, 2, \ldots, k$. That is, we find expression (4.167), $q_k(x) = \sum_{i=1}^{k} p_m(x)$, with

$$p_m(x) = \frac{2}{L} \sin^2\left(\frac{k\pi x}{L} - \pi(m-1)\right), \quad m = 1, 2, \ldots, k, \tag{4.176}$$

where in this case the λ_m's of expression (4.166) are taken as $(m-1)L/k$. Therefore, we conclude that the complexity is degenerated for all the energy eigenstates of the quantum infinite square well. Its value can be exactly calculated. Considering that L is the natural length unit in this problem, we obtain

$$C(p) = C(q_k) = \frac{3}{e} = 1.1036\ldots. \tag{4.177}$$

In the general case of a particle in a d-dimensional box of width L in each dimension, it can also be verified that complexity is degenerated for all its energy eigenstates with a constant value given by $C = (3/e)^d$.

Here we have shown that, in the same way that the complexity breaks the energy degeneration in the H-atom and in the quantum isotropic harmonic oscillator, the contrary behavior is also possible. In particular, the complexity is constant for the

whole energy spectrum of the d-dimensional quantum infinite square well. This result is due to the same functional form displayed by all the energy eigenstates of this system. Therefore, it suggests that the study of the statistical complexity in a quantum system allows to infer some properties on its structural conformation.

4.4.5 The Periodic Table

The use of these statistical magnitudes to study the electronic structure of atoms is another interesting application [64, 89, 143–148]. The basic ingredient to calculate these statistical indicators is the electron probability density, $\rho(\mathbf{r})$, that can be obtained from the numerically derived Hartree-Fock atomic wave function in the non-relativistic case [143, 144], and from the Dirac-Fock atomic wave function in the relativistic case [145]. The behavior of these statistical quantifiers with the atomic number Z has revealed a connection with physical measures, such as the ionization potential and the static dipole polarizability [89]. All of them, theoretical and physical magnitudes, are capable of unveiling the shell structure of atoms, specifically the closure of shells in the noble gases. Also, it has been observed that statistical complexity fluctuates around an average value that is non-decreasing as the atomic number Z increases in the non-relativistic case [144, 145]. This average value becomes increasing in the relativistic case [145]. This trend has also been confirmed when the atomic electron density is obtained with a different approach [149]. In another context where the main interactions have a gravitational origin, as it is the case of a white dwarf, it has also been observed that complexity grows as a function of the star mass, from the low-mass non-relativistic case to the extreme relativistic limit. In particular, complexity for the white dwarf reaches a maximum finite value in the Chandrasekhar limit as it was calculated by Sañudo and López-Ruiz [150].

An alternative method to calculate the statistical magnitudes can be used when the atom is seen as a discrete hierarchical organization. The atomic shell structure can also be captured by the fractional occupation probabilities of electrons in the different atomic orbitals. This set of probabilities is here employed to evaluate all these quantifiers for the non-relativistic (NR) and relativistic (R) cases. In the NR case, a non-decreasing trend in complexity as Z increases is obtained and also the closure of shells for some noble gases is observed [96, 151].

For the NR case, each electron shell of the atom is given by $(nl)^w$ [152], where n denotes the principal quantum number, l the orbital angular momentum ($0 \leq l \leq n-1$) and w is the number of electrons in the shell ($0 \leq w \leq 2(2l+1)$). For the R case, due to the spin-orbit interaction, each shell is split, in general, in two shells [153]: $(nlj_-)^{w_-}$, $(nlj_+)^{w_+}$, where $j_\pm = l \pm 1/2$ (for $l = 0$ only one value of j is possible, $j = j_+ = 1/2$) and $0 \leq w_\pm \leq 2j_\pm + 1$. As an example, we explicitly give the electron configuration of Ar($Z = 18$) in both cases,

$$\mathrm{Ar}(NR) : (1\mathrm{s})^2(2\mathrm{s})^2(2\mathrm{p})^6(3\mathrm{s})^2(3\mathrm{p})^6, \tag{4.178}$$

$$\mathrm{Ar}(R) : (1\mathrm{s}1/2)^2(2\mathrm{s}1/2)^2(2\mathrm{p}1/2)^2(2\mathrm{p}3/2)^4(3\mathrm{s}1/2)^2(3\mathrm{p}1/2)^2(3\mathrm{p}3/2)^4. \tag{4.179}$$

For each atom, a fractional occupation probability distribution of electrons in atomic orbitals $\{p_k\}$, $k = 1, 2, \ldots, \Pi$, being Π the number of shells of the atom, can be defined. This normalized probability distribution $\{p_k\}$ ($\sum p_k = 1$) is easily calculated by dividing the superscripts $w_\pm$ (number of electrons in each shell) by Z, the total number of electrons in neutral atoms, which is the case we are considering here. The order of shell filling dictated by nature [152] has been chosen. Then, from this probability distribution, the different statistical magnitudes (Shannon entropy, disequilibrium, statistical complexity and Fisher-Shannon entropy) is calculated.

In order to calculate the statistical complexity $C = H \cdot D$, with $H = e^S$, we use the discrete versions of the Shannon entropy S and disequilibrium D:

$$S = -\sum_{k=1}^{\Pi} p_k \log p_k, \tag{4.180}$$

$$D = \sum_{k=1}^{\Pi} (p_k - 1/\Pi)^2. \tag{4.181}$$

To compute the Fisher-Shannon information, $P = J \cdot I$, with $J = \frac{1}{2\pi e} e^{2S/3}$, the discrete version of I is defined as [96, 151]

$$I = \sum_{k=1}^{\Pi} \frac{(p_{k+1} - p_k)^2}{p_k}, \tag{4.182}$$

where $p_{\Pi+1} = 0$ is taken.

The statistical complexity, C, as a function of the atomic number, Z, for the NR and R cases for neutral atoms is given in Figs. 4.22 and 4.23, respectively. It is observed in both figures that this magnitude fluctuates around an increasing average value with Z. This increasing trend recovers the behavior obtained by using the continuous quantum-mechanical wave functions [144, 145]. A shell-like structure is also unveiled in this approach by looking at the minimum values of C taken on the noble gases positions (the dashed lines in the figures) with the exception of Ne($Z = 10$) and Ar($Z = 18$). This behavior can be interpreted as special arrangements in the atomic configuration for the noble gas cases out of the general increasing trend of C with Z.

The Fisher-Shannon entropy, P, as a function of Z, for the NR and R cases in neutral atoms is given in Figs. 4.24 and 4.25, respectively. The shell structure is again displayed in the special atomic arrangements, particularly in the R case (Fig. 4.25) where P takes local maxima for all the noble gases (see the dashed lines on $Z = 2$, 10, 18, 36, 54, 86). The irregular filling (i.f.) of s and d shells [152] is also detected by peaks in the magnitude P, mainly in the R case. In particular, see the elements Cr and Cu (i.f. of 4s and 3d shells); Nb, Mo, Ru, Rh, and Ag (i.f. of 5s and 4d shells); and finally Pt and Au (i.f. of 6s and 5d shells). Pd also has an irregular filling, but P does not display a peak on it because the shell filling in this case does not follow the same procedure as the before elements (the 5s shell is empty and the 5d is full). Finally, the increasing trend of P with Z is clearly observed.

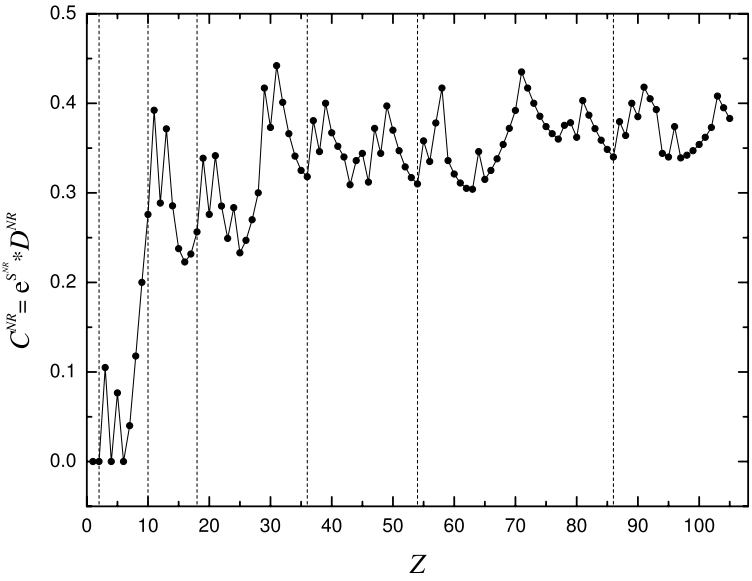

Fig. 4.22 Statistical complexity, C, vs. Z in the non relativistic case (C^{NR}). The *dashed lines* indicate the position of noble gases. For details, see the text

Then, it is found that P, the Fisher-Shannon entropy, in the relativistic case (Fig. 4.25) reflects in a clearer way the increasing trend with Z, the shell structure in noble gases, and the irregular shell filling of some specific elements. The same method that uses the fractional occupation probability distribution is applied in the next section to another many particle system, the atomic nucleus, that has also been described by a shell model.

4.4.6 Magic Numbers in Nuclei

Nucleus is another interesting quantum system that can be described by a shell model [154]. In this picture, just as electrons in atoms, nucleons in nuclei fill in the nuclear shells by following a determined hierarchy. Hence, the fractional occupation probabilities of nucleons in the different nuclear orbitals can capture the nuclear shell structure. This set of probabilities, as explained in the above section, can be used to evaluate the statistical quantifiers for nuclei as a function of the number of nucleons. In this section, by following this method, the calculation of statistical complexity and Fisher-Shannon information for nuclei is presented [155].

The nuclear shell model is developed by choosing an intermediate three-dimensional potential, between an infinite well and the harmonic oscillator, in which nucleons evolve under the Schrödinger equation with an additional spin-orbit interaction [154]. In this model, each nuclear shell is given by $(nlj)^w$, where l denotes

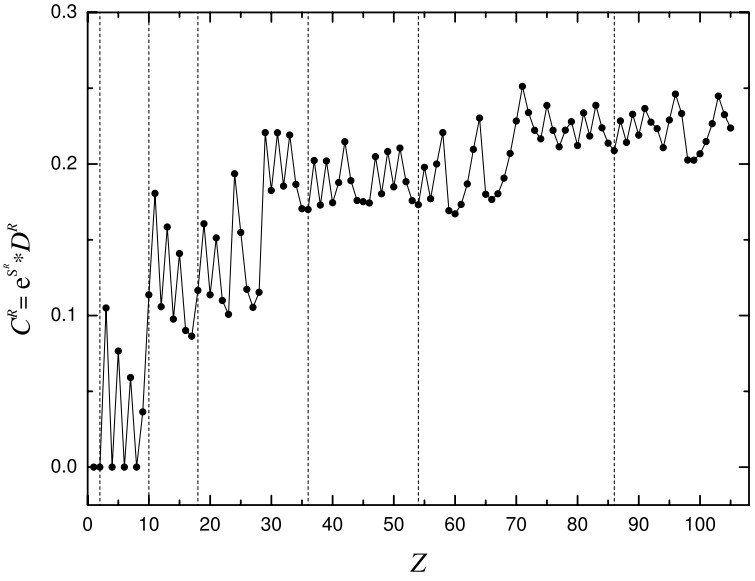

Fig. 4.23 Statistical complexity, C, vs. Z in the relativistic case (C^R). The comments given in Fig. 4.22 are also valid here

the orbital angular momentum ($l = 0, 1, 2, \ldots$), n counts the number of levels with that l value, j can take the values $l + 1/2$ and $l - 1/2$ (for $l = 0$ only one value of j is possible, $j = 1/2$), and w is the number of one-type of nucleons (protons or neutrons) in the shell ($0 \leq w \leq 2j + 1$).

As an example, we explicitly give the shell configuration of a nucleus formed by $Z = 20$ protons or by $N = 20$ neutrons. In both cases, it is obtained [154]:

$$\left\{ \begin{array}{l} (Z = 20) \\ (N = 20) \end{array} \right\} : (1s1/2)^2 (1p3/2)^4 (1p1/2)^2 (1d5/2)^6 (2s1/2)^2 (1d3/2)^4. \quad (4.183)$$

When one-type of nucleons (protons or neutrons) in the nucleus is considered, a fractional occupation probability distribution of this type of nucleons in nuclear orbitals $\{p_k\}$, $k = 1, 2, \ldots, \Pi$, being Π the number of shells for this type of nucleons, can be defined in the same way as it has been done for electronic calculations in the atom in the previous section. This normalized probability distribution $\{p_k\}$ ($\sum p_k = 1$) is easily found by dividing the superscripts w by the total of the corresponding type of nucleons (Z or N). Then, from this probability distribution, the different statistical magnitudes (Shannon entropy, disequilibrium, statistical complexity and Fisher-Shannon entropy) by following expressions (4.180–4.182) are obtained.

The statistical complexity, C, of nuclei as a function of the number of nucleons, Z or N, is given in Fig. 4.26. Here we can observe that this magnitude fluctuates around an increasing average value with Z or N. This trend is also found for the electronic structure of atoms (see previous section), reinforcing the idea that, in

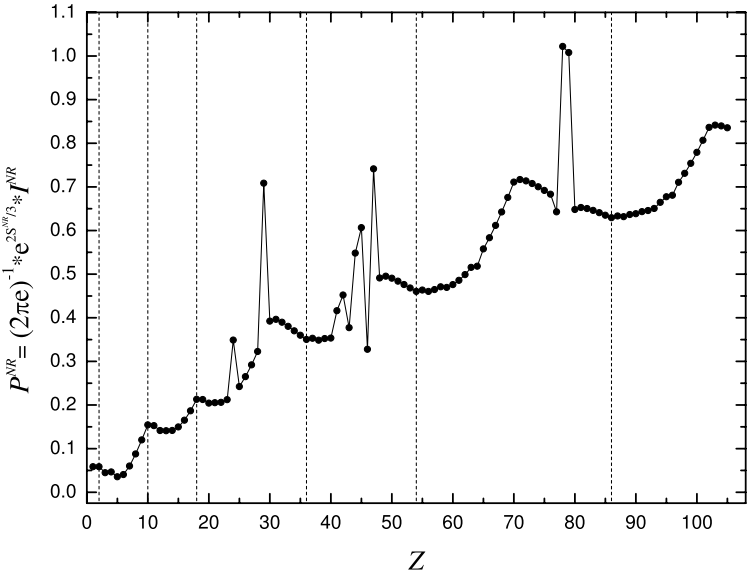

Fig. 4.24 Fisher-Shannon entropy, P, vs. Z, in the non relativistic case (P^{NR}). The *dashed lines* indicate the position of noble gases. For details, see the text

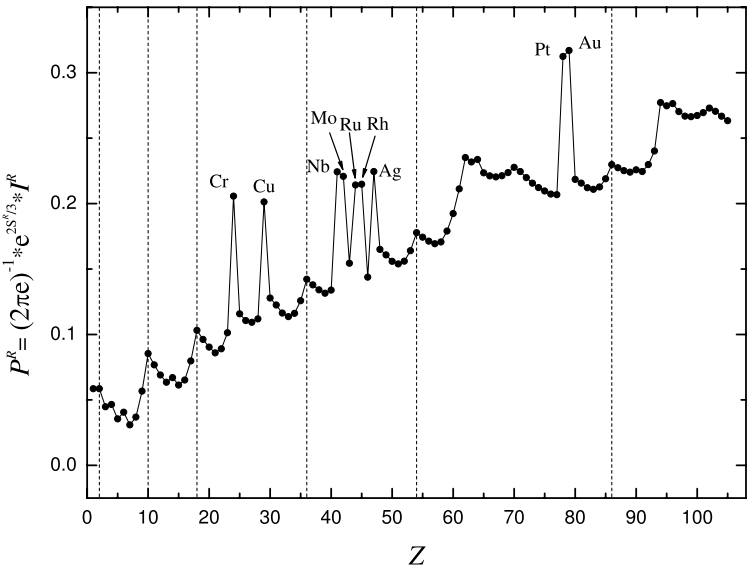

Fig. 4.25 Fisher-Shannon entropy, P, vs. Z, in the relativistic case (P^{R}). The comments given in Fig. 4.24 are also valid here

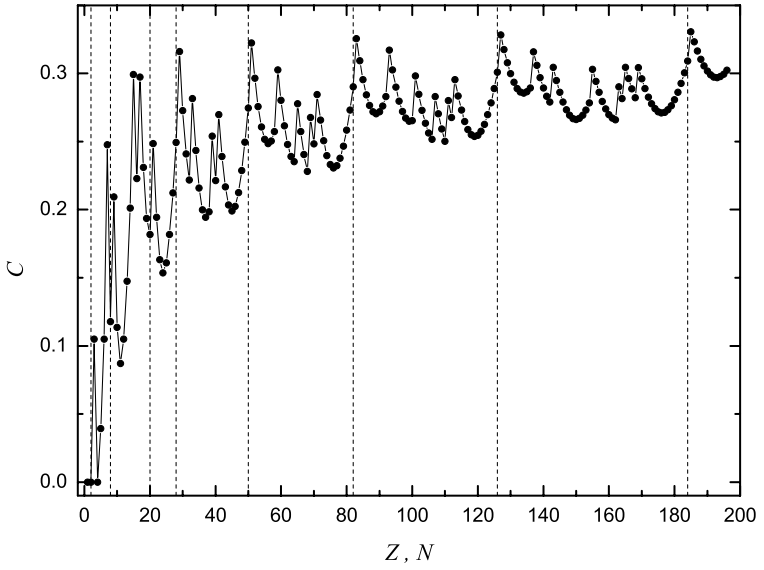

Fig. 4.26 Statistical complexity, C, vs. number of nucleons, Z or N. The *dashed lines* indicate the positions of magic numbers $\{2, 8, 20, 28, 50, 82, 126, 184\}$. For details, see the text

general, complexity increases with the number of units forming a system. However, the shell model supposes that the system encounters certain ordered rearrangements for some specific number of units (electrons or nucleons). This shell-like structure is also unveiled by C in this approach to nuclei. In this case, the extremal values of C are not taken just on the closed shells as happens in the noble gases positions for atoms, if not that they appear to be in the positions one unit less than the closed shells.

The Fisher-Shannon entropy, P, of nuclei as a function of Z or N is given in Fig. 4.27. It presents an increasing trend with Z or N. The spiky behavior of C provoked by the nuclear shell structure becomes smoother for P, that presents peaks (changes in the sign of the derivative) only at a few Z or N, concretely at the numbers 2, 6, 14, 20, 28, 50, 82, 126, 184. Strikingly, the sequence of magic numbers is $\{2, 8, 20, 28, 50, 82, 126, 184\}$ (represented as dashed vertical lines in the figures). Only the peaks at 6 and 14 disagree with the sequence of magic numbers, what could be justified by saying that statistical indicators work better for high numbers. But in this case, it should be observed that the carbon nucleus, $C^{N=6}_{Z=6}$, and the silicon nucleus, $Si^{N=14}_{Z=14}$, apart from their great importance in nature and industry, they are the stable isotopes with the greatest abundance in the corresponding isotopic series, 98.9% and 92.2%, respectively.

Then, the increasing trend of these statistical magnitudes with Z or N, and the reflect of the shell structure in the spiky behavior of their plots are found when using for their calculation the fractional occupation probability distribution of nucleons, Z or N. It is worth to note that the relevant peaks in the Fisher-Shannon information

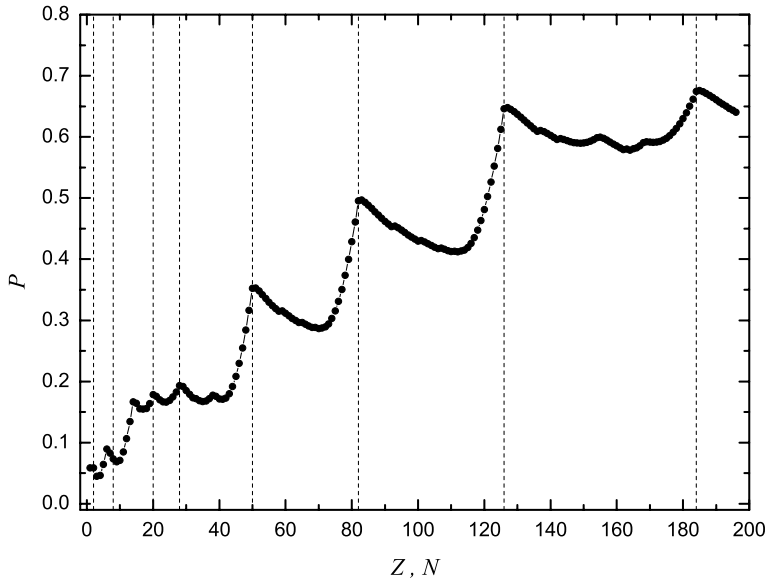

Fig. 4.27 Fisher-Shannon entropy, P, vs. the number of nucleons, Z or N. The *dashed lines* indicate the positions of magic numbers {2, 8, 20, 28, 50, 82, 126, 184}. For details, see the text

are revealed to be just the series of magic numbers in nuclei. This fact indicates again that these statistical indicators are able to enlighten some structural aspects of quantum many-body systems.

Acknowledgements R.L.-R. thanks Prof. Sen for his invitation to prepare and to present this chapter in this book.

References

1. Hawking S (2000) I think the next century will be the century of complexity. San José Mercury News, Morning Final Edition, January 23
2. Anderson PW (1991) Is complexity physics? Is it science? What is it? Phys Today 9–11, July
3. Parisi G (1993) Statistical physics and biology. Phys World 6:42–47
4. Shannon CE, Weaver W (1949) The mathematical theory of communication. University of Illinois Press, Urbana
5. Nicolis G, Prigogine I (1977) Self-organization in nonequilibrium systems. Wiley, New York
6. López-Ruiz R (1994) On instabilities and complexity. PhD thesis, Universidad de Navarra, Pamplona
7. López-Ruiz R, Mancini HL, Calbet X (1995) A statistical measure of complexity. Phys Lett A 209:321–326
8. Kolmogorov AN (1965) Three approaches to the definition of quantity of information. Probl Inf Transm 1:3–11
9. Chaitin GJ (1966) On the length of programs for computing finite binary sequences. J Assoc Comput Mach 13:547–569

10. Chaitin GJ (1990) Information, randomness & incompleteness. World Scientific, Singapore
11. Lempel A, Ziv J (1976) On the complexity of finite sequences. IEEE Trans Inf Theory 22:75–81
12. Bennett CH (1985) Information, dissipation, and the definition of organization. In: Pines D (ed) Emerging syntheses in science. Santa Fe Institute, Santa Fe, pp 297–313
13. Grassberger P (1986) Toward a quantitative theory of self-generated complexity. Int J Theor Phys 25:907–938
14. Huberman BA, Hogg T (1986) Complexity and adaptation. Physica D 22:376–384
15. Loyd S, Pagels H (1988) Complexity as thermodynamic depth. Ann Phys (NY) 188:186–213
16. Crutchfield JP, Young K (1989) Inferring statistical complexity. Phys Rev Lett 63:105–108
17. Adami C, Cerf NT (2000) Physical complexity of symbolic sequences. Physica D 137:62–69
18. Sánchez JR, López-Ruiz R (2005) A method to discern complexity in two-dimensional patterns generated by coupled map lattices. Physica A 355:633–640
19. Calbet X, López-Ruiz R (2001) Tendency toward maximum complexity in a non-equilibrium isolated system. Phys Rev E 63:066116 (9 pp)
20. Escalona-Morán M, Cosenza MG, López-Ruiz R, García P (2010) Statistical complexity and nontrivial collective behavior in electroencephalographic signals. Int J Bifurc Chaos 20:1723–1729. Special issue on Chaos and dynamics in biological networks, Eds Chávez & Cazelles
21. Feldman DP, Crutchfield JP (1998) Measures of statistical complexity: Why? Phys Lett A 238:244–252
22. Lin J (1991) Divergence measures based on the Shannon entropy. IEEE Trans Inf Theory 37:145–151
23. Martín MT, Plastino A, Rosso OA (2003) Statistical complexity and disequilibrium. Phys Lett A 311:126–132
24. Lamberti W, Martín MT, Plastino A, Rosso OA (2004) Intensive entropic non-triviality measure. Physica A 334:119–131
25. Feng G, Song S, Li P (1998) A statistical measure of complexity in hydrological systems. J Hydrol Eng Chin (Hydrol Eng Soc) 11:14
26. Shiner JS, Davison M, Landsberg PT (1999) Simple measure for complexity. Phys Rev E 59:1459–1464
27. Yu Z, Chen G (2000) Rescaled range and transition matrix analysis of DNA sequences. Commun Theor Phys (Beijing, China) 33:673–678
28. Rosso OA, Martín MT, Plastino A (2003) Tsallis non-extensivity and complexity measures. Physica A 320:497–511
29. Rosso OA, Martín MT, Plastino A (2005) Evidence of self-organization in brain electrical activity using wavelet-based informational tools. Physica A 347:444–464
30. Lovallo M, Lapenna V, Telesca L (2005) Transition matrix analysis of earthquake magnitude sequences. Chaos Solitons Fractals 24:33–43
31. López-Ruiz R (2005) Shannon information, LMC complexity and Rényi entropies: a straightforward approach. Biophys Chem 115:215
32. Pomeau Y, Manneville P (1980) Intermittent transition to turbulence in dissipative dynamical systems. Commun Math Phys 74:189–197
33. Chaté H, Manneville P (1987) Transition to turbulence via spatio-temporal intermittency. Phys Rev Lett 58:112–115
34. Houlrik JM, Webman I, Jensen MH (1990) Mean-field theory and critical behavior of coupled map lattices. Phys Rev A 41:4210–4222
35. Rolf J, Bohr T, Jensen MH (1998) Directed percolation universality in asynchronous evolution of spatiotemporal intermittency. Phys Rev E 57:R2503–R2506
36. Argentina M, Coullet P (1997) Chaotic nucleation of metastable domains. Phys Rev E 56:R2359–R2362
37. Zimmermann MG, Toral R, Piro O, San Miguel M (2000) Stochastic spatiotemporal intermittency and noise-induced transition to an absorbing phase. Phys Rev Lett 85:3612–3615
38. Pomeau Y (1986) Front motion, metastability and subcritical bifurcations in hydrodynamics. Physica D 23:3–11

39. Menon GI, Sinha S, Ray P (2003) Persistence at the onset of spatio-temporal intermittency in coupled map lattices. Europhys Lett 61:27–33
40. López-Ruiz R, Fournier-Prunaret D (2004) Complex behaviour in a discrete logistic model for the symbiotic interaction of two species. Math Biosci Eng 1:307–324
41. López-Ruiz R, Fournier-Prunaret D (2008) Logistic models for symbiosis, predator-prey and competition. In: Encyclopedia of networked and virtual organization, vol II, pp 838–847. Also presented at Conference 'Verhulst 200 on Chaos', abstracts, p 56, Royal Military Academy, Brussels (2004)
42. McKay CP (2004) What is life? PLoS Biol 2:1260–1263
43. Sánchez JR, López-Ruiz R (2005) Detecting synchronization in spatially extended discrete systems by complexity measurements. Discrete Dyn Nat Soc 9:337–342
44. Kolmogorov AN (1958) A new metric invariant of transitive dynamical systems and automorphisms of Lebesgue spaces. Dokl Akad Nauk SSSR 119:861–864
45. Sinai JG (1959) On the concept of entropy of a dynamical system. Dokl Akad Nauk SSSR 124:768–771
46. Landsberg PT, Shiner JS (1998) Disorder and complexity in an ideal non-equilibrium Fermi gas. Phys Lett A 245:228–232
47. Atmanspacher H, Räth C, Wiedermann G (1997) Statistics and meta-statistics in the concept of complexity. Physica A 234:819–829
48. Gell-Mann M (1995) What is complexity. Complexity 1:16–19
49. Anteneodo C, Plastino AR (1996) Some features of the statistical LMC complexity. Phys Lett A 223:348–354
50. Latora V, Baranger M (1999) Kolmogorov-Sinai entropy rate versus physical entropy. Phys Rev Lett 82:520–523
51. Calbet X, López-Ruiz R (2007) Extremum complexity distribution of a monodimensional ideal gas out of equilibrium. Physica A 382:523–530
52. Calbet X, López-Ruiz R (2009) Extremum complexity in the monodimensional ideal gas: the piecewise uniform density distribution approximation. Physica A 388:4364–4378
53. López-Ruiz R (2001) Complexity in some physical systems. Int J Bifurc Chaos 11:2669–2673
54. Catalán RG, Garay J, López-Ruiz R (2002) Features of the extension of a statistical measure of complexity to continuous systems. Phys Rev E 66:011102 (6 pp)
55. Romera E, López-Ruiz R, Sañudo Nagy Á (2009) Generalized statistical complexity and Fisher-Rényi entropy product in the H-atom. Int Rev Phys (IREPHY) 3:207–211
56. López-Ruiz R, Nagy Á, Romera E, Sañudo J (2009) A generalized statistical complexity measure: Applications to quantum systems. J Math Phys 50:123528(10)
57. Khinchin AI (1957) Mathematical foundations of information theory. Dover, New York
58. Wehrl A (1978) General properties of entropy. Rev Mod Phys 50:221–260
59. Tsallis C, Mendes RS, Plastino AR (1998) The role of constraints within generalized nonextensive statistics. Physica A 261:534–554
60. Dembo A, Cover TM, Thomas JA (1991) Information theoretic inequalities. IEEE Trans Inf Theory 37:1501–1518
61. Gadre SR (1984) Information entropy and Thomas-Fermi theory. Phys Rev A 30:620–621
62. Gadre SR, Bendale RD (1985) Maximization of atomic information-entropy sum in configuration and momentum spaces. Int J Quant Chem 28:311–314
63. Gadre SR, Bendale RD (1985) Information entropies in quantum-chemistry. Curr Sci (India) 54:970–977
64. Gadre SR, Sears SB, Chakravorty SJ, Bendale RD (1985) Some novel characteristics of atomic information entropies. Phys Rev A 32:2602–2606
65. Gadre SR, Bendale RD (1987) Rigorous relationships among quantum-mechanical kinetic energy and atomic information entropies: Upper and lower bounds. Phys Rev A 36:1932–1935
66. Shannon CE (1948) A mathematical theory of communication. Bell Syst Tech J 27:379–423
67. Fisher RA (1925) Theory of statistical estimation. Proc Camb Philos Soc 22:700–725
68. Esquivel RO, Rodriguez AL, Sagar RP, Smith VH Jr (1996) Physical interpretation of information entropy: Numerical evidence of the Collins conjecture. Phys Rev A 54:259–265

69. Massen SE, Panos CP (1998) Universal property of the information entropy in atoms, nuclei and atomic clusters. Phys Lett A 246:530–533
70. Massen SE, Panos CP (2001) A link of information entropy and kinetic energy for quantum many-body systems. Phys Lett A 280:65–69
71. Sagar RP, Ramirez JC, Esquivel RO, Ho M Jr (2002) Relationships between Jaynes entropy of the one-particle density matrix and Shannon entropy of the electron densities. J Chem Phys 116:9213–9221
72. Nalewajski RF, Switka E, Michalak A (2002) Information distance analysis of molecular electron densities. Int J Quant Chem 87:198–213
73. Nagy Á (2003) Spin virial theorem in the time-dependent density-functional theory. J Chem Phys 119:9401–9405
74. Massen SE (2003) Application of information entropy to nuclei. Phys Rev C 67:014314 (7 pp)
75. Nalewajski RF (2003) Information principles in the theory of electronic structure. Chem Phys Lett 372:28–34
76. Nalewajski RF (2003) Information principles in the loge theory. Chem Phys Lett 375:196–203
77. Romera E, Dehesa JS (2004) The Fisher-Shannon information plane, an electron correlation tool. J Chem Phys 120:8906–8912
78. Parr RG, Ayers PW, Nalewajski RF (2005) What is an atom in a molecule? J Phys Chem A 109:3957–3959
79. Sen KD (2005) N-derivative of Shannon entropy of shape function for atoms. J Chem Phys 123:074110 (9 pp)
80. Guevara NL, Sagar RP, Esquivel RO (2005) Local correlation measures in atomic systems. J Chem Phys 122:084101
81. Sagar RP, Guevara NL (2005) Local correlation measures in atomic systems. J Chem Phys 123:044108 (10 pp)
82. Romera E, Sánchez-Moreno P, Dehesa JS (2005) The Fisher information of single-particle systems with a central potential. Chem Phys Lett 414:468–472
83. Nagy Á (2006) Fisher information in a two-electron entangled artificial atom. Chem Phys Lett 425:154–156
84. Nagy Á, Sen KD (2006) Atomic Fisher information versus atomic number. Phys Lett A 360:291–293
85. Sagar RP, Guevara NL (2006) Mutual information and electron correlation in momentum space. J Chem Phys 124:134101 (9 pp)
86. Sen KD, Katriel J (2006) Information entropies for eigendensities of homogeneous potentials. J Chem Phys 125:074117 (4 pp)
87. Nagy Á (2007) Fisher information and Steric effect. Chem Phys Lett 449:212–215
88. Liu S (2007) On the relationship between densities of Shannon entropy and Fisher information for atoms and molecules. J Chem Phys 126:191107 (3 pp)
89. Sen KD, Panos CP, Chatzisavas KCh, Moustakidis ChC (2007) Net Fisher information measure versus ionization potential and dipole polarizability in atoms. Phys Lett A 364:286–290
90. Patil SH, Sen KD, Watson NA, Montgomery HE Jr (2007) Characteristic features of net information measures for constrained Coulomb potentials. J Phys B 40:2147–2162
91. Sagar RP, Guevara NL (2008) Relative entropy and atomic structure. J Mol Struct, Theochem 857:72–77
92. Nagy Á, Liu S (2008) Local wave-vector, Shannon and Fisher information. Phys Lett A 372:1654–1656
93. Sañudo, López-Ruiz R (2008) Some features of the statistical complexity, Fisher-Shannon information and Bohr-like orbits in the quantum isotropic harmonic oscillator. J Phys A, Math Theor 41:265303 (7 pp)
94. Sañudo J, López-Ruiz R (2008) Statistical complexity and Fisher-Shannon information in the H-atom. Phys Lett A 372:5283–5286

95. Seo DK, Weng CJ (2008) Orbital interpretation of kinetic energy density and a direct space comparison of chemical bonding in tetrahedral network solids. Phys Chem A 112:7705–7716
96. Sañudo J, López-Ruiz R (2009) Alternative evaluation of statistical indicators in atoms: The non-relativistic and relativistic cases. Phys Lett A 373:2549–2551
97. Nalewajski RF (2009) Entropic descriptors of the chemical bond in H_2: local resolution of stockholder atoms. J Math Chem 45:1041–1054
98. Parr RG, Yang W (1989) Density functional theory of atoms and molecules. Oxford University Press, New York
99. Szabo JB, Sen KD, Nagy Á (2008) The Fisher-Shannon information plane for atoms. Phys Lett A 372:2428–2430
100. Montgomery HE Jr, Sen KD (2008) Statistical complexity and Fisher-Shannon information measure of H_2^+. Phys Lett A 372:2271–2273
101. Mitnik DM, Randazzo J, Gasaneo G (2008) Endohedrally confined helium: Study of mirror collapses. Phys Rev A 78:062501 (10 pp)
102. Romera E (2002) Stam's principle D-dimensional uncertainty-like relationships and some atomic properties. Mol Phys 100:3325–3329
103. Romera E, Sánchez-Moreno P, Dehesa JS (2006) Uncertainty relation for Fisher information of D-dimensional single-particle systems with central potentials. J Math Phys 47:103504 (11 pp)
104. Hall MJW (2000) Quantum properties of classical Fisher information. Phys Rev A 62:012107
105. Hall MJW (2001) Exact uncertainty relations. Phys Rev A 64:052103
106. Hall MJW, Reginatto M (2002) Schrödinger equation from an exact uncertainty principle. J Phys A 35:3289–3302
107. Hall MJW (2004) Prior information: How to circumvent the standard joint-measurement uncertainty relation. Phys Rev A 69:052113
108. Luo S (2000) Quantum Fisher information and uncertainty relations. Lett Math Phys 53:243–251
109. Luo S (2003) Wigner-Yanase skew information and uncertainty relations. Phys Rev Lett 91:180403
110. Luo S, Zhang Z (2004) An informational characterization of Schrödinger's uncertainty relation. J Stat Phys 114:1557–1576
111. Petz D (2003) Covariance and Fisher information in quantum mechanics. J Phys A 35:79–91
112. Romera E, Angulo JC, Dehesa JS (1999) Fisher entropy and uncertainty-like relationships in many-body systems. Phys Rev A 59:4064–4067
113. Stam A (1959) Some inequalities satisfied by the quantities of information of Fisher and Shannon. Inf Control 2:101–112
114. Rao CR (1965) Linear statistical interference and its applications. Wiley, New York
115. Romera E, Dehesa JS (1994) Weizsäcker energy of many-electron systems. Phys Rev A 50:256–266
116. Bialynicki-Birula I, Mycielski J (1975) Uncertainty relations for information entropy in wave mechanics. Commun Math Phys 44:129–132
117. Carlen EA (1991) Superadditivity of Fisher's information and logarithmic Sobolev inequalities. J Funct Anal 101:194–211
118. Fulde P (1995) Electron correlation in molecules and solids. Springer, Berlin
119. Kutzelnigg W, del Re G, Berthier G (1968) Correlation coefficients for electronic wave functions. Phys Rev 172:49–59
120. Grassi A (2008) A relationship between atomic correlation energy and Tsallis entropy. Int J Quant Chem 108:774–778
121. Collins DM (1993) Entropy maximizations on electron-density. Z Naturforsch 48Z:68–74
122. Grassi A, Lombardo GM, March NH, Pucci R (1998) $1/Z$ expansion, correlation energy, and Shannon entropy of heavy atoms in nonrelativistic limit. Int J Quant Chem 69:721–726
123. Mohareji A, Alipour M (2009) Shannon information entropy of fractional occupation probability as an electron correlation measure in atoms and molecules. Chem Phys 360:132–136

124. Guevara NL, Sagar RP, Esquivel RO (2003) Shannon-information entropy sum as a correlation measure in atomic systems. Phys Rev A 67:012507
125. Sagar RP, Laguna HG, Guevara NL (2009) Conditional entropies and position-momentum correlations in atomic systems. Mol Phys 107:2071–2080
126. Ziesche P, Smigh VH Jr, Ho M, Rudin SP, Gersdorfand P, Taut M (1999) The He isoelectronic series and the Hooke's law model: Correlation measures and modifications of Collins' conjecture. J Chem Phys 110:6135–6142
127. Huang Z, Kais S (2005) Entanglement as measure of electron-electron correlation in quantum chemistry calculations. Chem Phys Lett 413:1–5
128. Gottlieb AD, Mauser NJ (2005) New measure of electron correlation. Phys Rev Lett 95:123003 (4 pp)
129. Juhász T, Mazziotti DA (2006) The cumulant two-particle reduced density matrix as a measure of electron correlation and entanglement. J Chem Phys 125:174105 (5 pp)
130. Amovilli C, March NH (2004) Quantum information: Jaynes and Shannon entropies in a two-electron entangled artificial atom. Phys Rev A 69:054302 (4 pp)
131. Koga T, Kasai Y, Thakkar AJ (1993) Accurate algebraic densities and intracules for helium-like ions. Int J Quant Chem 46:689–699
132. Taut M (1993) Two electrons in an external oscillator potential: Particular analytic solutions of a Coulomb correlation problem. Phys Rev A 48:3561–3566
133. Cioslowski J, Pernal K (2000) The ground state of harmonium. J Chem Phys 113:8434–8443
134. Landau LD, Lifshitz LM (1981) Quantum mechanics: non-relativistic theory, 3rd edn, vol 3. Butterworth-Heinemann, Oxford
135. Galindo A, Pascual P (1991) Quantum mechanics I. Springer, Berlin
136. Bethe HA, Salpeter EE (1977) Quantum mechanics of one-and two-electron atoms. Springer, Berlin
137. Eisberg JL (1961) Fundamentals of modern physics. Wiley, New York
138. Lebedev VS, Beigman IL (1998) Physics of highly excited atoms and ions. Springer, Berlin
139. Coffey MW (2003) Semiclassical position entropy for hydrogen-like atoms. J Phys A, Math Gen 36:7441–7448
140. Yánez RJ, van Assche W, Dehesa JS (1994) Position and momentum information entropies of the D-dimensional harmonic oscillator and hydrogen atom. Phys Rev A 50:3065–3079
141. López-Ruiz R, Sañudo J (2009) Complexity invariance by replication in the quantum square well. Open Syst Inf Dyn 16:423–427
142. Cohen-Tannoudji C, Diu B, Laloë F (1977) Quantum mechanics. Wiley, New York. 2 vols
143. Chatzisavvas KCh, Moustakidis ChC, Panos CP (2005) Information entropy, information distances, and complexity in atoms. J Chem Phys 123:174111 (10 pp)
144. Panos CP, Chatzisavvas KCh, Moustakidis ChC, Kyrkou EG (2007) Comparison of SDL and LMC measures of complexity: Atoms as a testbed. Phys Lett A 363:78–83
145. Borgoo A, De Proft F, Geerlings P, Sen KD (2007) Complexity of Dirac-Fock atom increases with atomic number. Chem Phys Lett 444:186–191
146. Angulo JC, Antolín J (2008) Atomic complexity measures in position and momentum spaces. J Chem Phys 128:164109 (7 pp)
147. Romera E, Nagy Á (2008) Rényi information of atoms. Phys Lett A 372:4918–4922
148. Borgoo A, Geerlings P, Sen KD (2008) Electron density and Fisher information of Dirac-Fock atoms. Phys Lett A 372:5106–5109
149. Sañudo J, López-Ruiz R (2008) Complexity in atoms: An approach with a new analytical density. Int Rev Phys (IREPHY) 2:223–230
150. Sañudo J, Pacheco AF (2009) Complexity and white-dwarf structure. Phys Lett A 373:807–810
151. Panos CP, Nikolaidis NS, Chatzisavvas KCh, Tsouros CC (2009) A simple method for the evaluation of the information content and complexity in atoms. A proposal for scalability. Phys Lett A 373:2343–2350
152. Bransden BH, Joachain CJ (2003) Physics of atoms and molecules, 2nd edn. Prentice Hall, London

153. Cowan RD (1981) The theory of atomic structure and spectra. University of California Press, Berkeley
154. Krane KS (1988) Introductory nuclear physics. Wiley, New York
155. López-Ruiz R, Sañudo J (2010) Evidence of magic numbers in nuclei by statistical indicators. Open Syst Inf Dyn 17:279–286